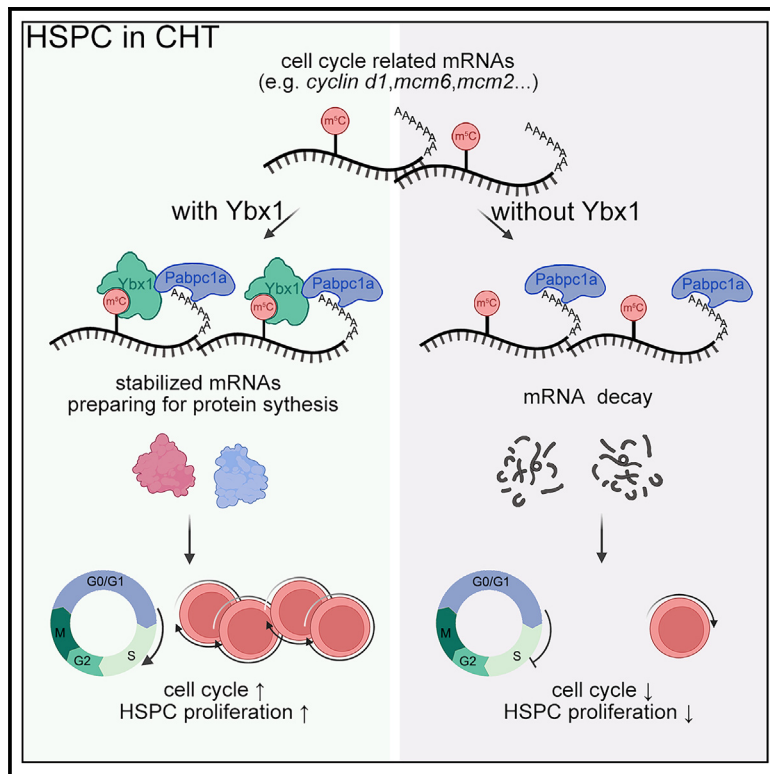


RNA m⁵C methylation mediated by Ybx1 ensures hematopoietic stem and progenitor cell expansion

Graphical abstract



Authors

Fan Liu, Mengke Wang, Suwei Gao, ..., Feng Liu, Ying Yang, Lu Wang

Correspondence

ygyang@big.ac.cn (Y.-G.Y.),
liuf@sdu.edu.cn (F.L.),
yingyang@big.ac.cn (Y.Y.),
wanglu1@ihcams.ac.cn (L.W.)

In brief

Liu et al. present a comprehensive view of the mRNA m⁵C landscapes during HSPC developmental switches and show that Ybx1 cooperates with Pabpc1a to maintain the stability of m⁵C-modified mRNAs, thereby ensuring proper HSPC expansion. Deletion of Ybx1 significantly inhibits HSPC proliferation.

Highlights

- Dynamic transcriptomic m⁵C landscapes during HSPC developmental switches in zebrafish
- m⁵C modification is essential for HSPC expansion through maintaining RNA stability
- Ybx1 is required for HSPC expansion by regulating m⁵C-modified cell-cycle-related mRNAs
- Ybx1 plays a crucial role in the expansion of mouse fetal liver HSPCs



Article

RNA m⁵C methylation mediated by Ybx1 ensures hematopoietic stem and progenitor cell expansion

Fan Liu,^{1,9} Mengke Wang,^{2,3,4,9} Suwei Gao,^{5,9} Gege Song,^{2,3,4} Mengyao Liu,¹ Ying Li,¹ Piao Sun,¹ Weiyi Lai,⁶ Hailin Wang,⁶ Yun-Gui Yang,^{2,3,4,*} Feng Liu,^{5,7,*} Ying Yang,^{2,3,4,*} and Lu Wang^{1,8,10,*}

¹State Key Laboratory of Experimental Hematology, National Clinical Research Center for Blood Diseases, Haihe Laboratory of Cell Ecosystem, Institute of Hematology & Blood Diseases Hospital, Chinese Academy of Medical Sciences & Peking Union Medical College, Tianjin 300020, China

²Beijing Institute of Genomics, Chinese Academy of Sciences and China National Center for Bioinformation, Beijing 100101, China

³Institute of Stem Cell and Regeneration, Chinese Academy of Sciences, Beijing 100101, China

⁴Sino-Danish College, University of Chinese Academy of Sciences, Beijing 100049, China

⁵Shandong Provincial Key Laboratory of Animal Cell and Developmental Biology, School of Life Sciences, Shandong University, Qingdao 266237, China

⁶State Key Laboratory of Environmental Chemistry and Ecotoxicology, Research Center for Eco-Environmental Sciences, Chinese Academy of Sciences, Beijing 100085, China

⁷State Key Laboratory of Membrane Biology, Institute of Zoology, Institute for Stem Cell and Regeneration, Chinese Academy of Sciences, University of Chinese Academy of Sciences, Beijing 100101, China

⁸Tianjin Institutes of Health Science, Tianjin 301600, China

⁹These authors contributed equally

¹⁰Lead contact

*Correspondence: ygyang@big.ac.cn (Y.-G.Y.), liuf@sdu.edu.cn (F.L.), yingyang@big.ac.cn (Y.Y.), wanglu1@ihcams.ac.cn (L.W.)
<https://doi.org/10.1016/j.celrep.2025.115324>

SUMMARY

Hematopoietic stem and progenitor cells (HSPCs) undergo rapid transcriptional transitions among distinct cell states and functional properties during development, but the underlying molecular mechanism is largely unknown. Here, we characterize the mRNA m⁵C landscape of developing HSPCs in zebrafish and found that m⁵C modification is essential for HSPC expansion through maintaining mRNA stability. Deletion of the m⁵C reader, Y-box binding protein 1 (Ybx1), significantly inhibits the proliferation of HSPCs in zebrafish and mice. Mechanistically, Ybx1 recognizes m⁵C-modified mRNAs and maintains the stability of cell-cycle-related transcripts, thereby ensuring proper HSPC expansion. This study reveals the critical role of Ybx1-mediated mRNA m⁵C modification in developmental hematopoiesis and provides new insights and epitranscriptomic strategies for optimizing HSPC expansion.

INTRODUCTION

Hematopoietic stem and progenitor cells (HSPCs) are a type of adult tissue stem cell that supports the lifelong supply of blood cells in vertebrates.^{1,2} The earliest and most primitive HSPCs, known as nascent HSPCs, originate from the aorta-gonad-mesonephros (AGM) region via a process of endothelial-to-hematopoietic transition (EHT),^{3–5} which then undergo a period of expansion, maturation, and differentiation in the fetal liver (FL) in mammals⁶ or the caudal hematopoietic tissue (CHT) region in zebrafish.^{7,8} Finally, HSPCs colonize into the bone marrow (BM) of mammals or the kidney marrow (KM) of zebrafish for lifelong maintenance of hematopoiesis.^{9,10} HSPCs undergo dynamic transitions in terms of cell states and functional properties during development. Most AGM-derived HSPCs are immature and subsequently migrate to the next hematopoietic tissues, while FL (or CHT)-resident HSPCs have the ability to mature and expand rapidly, and BM (or KM)-colonized HSPCs support homeostatic blood production. The developmental switches

involve substantial global transcriptional shifts, but the molecular mechanism underlying the large-scale transcriptome reprogramming is unclear.

The chemical modifications of RNAs have been increasingly recognized as a crucial layer of transcriptome regulation.^{11–13} 5-Methylcytosine (m⁵C), one of the most prevalent RNA modifications, involves the methylation of the fifth carbon of cytosine.¹⁴ The installation and removal of m⁵C modification are catalyzed by the methyltransferases (writers, NSUN family members) and demethylases (erasers, TET family members), respectively.^{15–19} Several RNA binding proteins (readers), such as ALYREF, YBX1, YBX2, and SRSF2, have been identified to preferentially recognize m⁵C sites and mediate the regulation of mRNA metabolism, thus participating in various biological processes, including mRNA export, stability, and splicing.^{15,16,20–26} Moreover, m⁵C plays a particularly important role in developmental contexts that require rapid shifts in the global transcriptional program, such as in maternal-to-zygotic transition, as we previously reported.²² Given the importance of m⁵C in transcriptome



regulation, we sought to explore its potential role in HSPC development.

In this study, we illustrate the landscapes of m⁵C modification in zebrafish HSPCs at different developmental stages. Our findings underscore the importance of m⁵C modification in HSPC expansion through maintaining RNA stability. Ybx1 preferentially binds to critical cell-cycle-related mRNAs containing m⁵C and recruits Pabpc1a to prevent their decay, thereby facilitating HSPC expansion. This study sheds light on a pivotal mechanism through which m⁵C modification regulates gene expression during HSPC development.

RESULTS

Dynamic transcriptomic landscapes of m⁵C modification during HSPC development

To elucidate the distinct characteristics of mRNA m⁵C modification during HSPC development, we conducted RNA bisulfite sequencing (RNA-BisSeq) and corresponding RNA sequencing (RNA-seq) on sorted HSPCs from three distinct development stages of zebrafish transgenic lines (*CD41:GFP*) and (*runx1:en-GFP*), including AGM-derived HSPCs at 33 h postfertilization (hpf), CHT-resident HSPCs at 52 hpf, and KM-colonized HSPCs at 12 months postfertilization (mpf) (Figures 1A, S1A, and S1B). The correlation between m⁵C methylation level and the read coverage indicated that the m⁵C methylation level was not influenced by the coverage changes (Figure S1C). mRNA m⁵C sites in HSPCs are predominantly located in coding sequence (CDS) regions (Figures S1D and S1E), consistent with previously reported m⁵C distribution in zebrafish.²² Notably, compared to AGM-derived HSPCs and KM-colonized HSPCs, the global m⁵C methylation levels at both site and mRNA levels in CHT-resident HSPCs were significantly increased (Figure 1B).

To further explore the role of m⁵C in developmental hematopoiesis, we categorized m⁵C-modified mRNAs from three stages into six clusters based on their methylation level (Figure 1C). Gene Ontology (GO) analysis revealed categories consistent with the characteristics of HSPCs at different developmental stages. For instance, hypermethylated mRNAs in AGM-derived HSPCs (cluster 1) were associated with functions related to the behavior of HSPCs as they bud and migrate into CHT from AGM. In CHT-resident HSPCs (cluster 3), m⁵C-modified mRNAs were enriched in cell-cycle-related functions, consistent with the rapid expansion of HSPCs at this stage. Cluster 5 displayed specific hypermethylation in KM-colonized HSPCs, and the enrichment of hematopoiesis- and stimulatory response-related terms corresponds to the homeostatic maintenance by the adult HSPCs. Clusters 2 and 4 included hypermethylated mRNAs that were common in the AGM-derived HSPCs and CHT-resident HSPCs or in the CHT-resident HSPCs and KM-colonized HSPCs, respectively. Further analysis revealed differentially methylated (DM) mRNAs between two stages (CHT-resident HSPCs vs. AGM-derived HSPCs and KM-colonized HSPCs vs. CHT-resident HSPCs) (Figure 1D). Between CHT-resident HSPCs and AGM-derived HSPCs, there were 962 up-methylated DM-mRNAs compared to 449 down-methylated, while the numbers were comparable (805 vs. 867) between KM-colonized and CHT-resident HSPCs (Figure 1D). The up-methylated

mRNAs in CHT-resident HSPCs (vs. AGM-derived HSPCs) were associated with functional categories for HSPC expansion (Figure 1E). Meanwhile, mRNAs with increased methylation levels in KM-colonized HSPCs (vs. CHT-resident HSPCs) were enriched for GO terms such as “interleukin receptor SHC signaling,” “cellular senescence,” and “hemostasis” (Figure 1F), corroborating the phenotypic characteristics. Collectively, these findings suggest that transcripts associated with stage-specific functions are preferably modified by m⁵C during HSPC development.

Next, we sought to explore the correlation between transcriptional changes and m⁵C modifications during HSPC development. The expression abundance changes of DM-mRNAs between adjacent developmental stages were analyzed. Pearson correlation analysis revealed high reproducibility of RNA-seq data (Figures S1F and S1G). Cumulative distribution function showed that the mRNA abundance changes (from AGM-derived HSPC to CHT-resident HSPC) in the up-methylated category were markedly less than those in the down-methylated category ($p = 6.06 \times 10^{-14}$) (Figure 1G), suggesting the mRNAs with up-regulated m⁵C levels are prevented from decaying. However, no significant mRNA abundance changes were observed between up- and down-methylated mRNAs from CHT-resident HSPCs to KM-colonized HSPCs (Figure S1H). Therefore, we hypothesized that m⁵C might play a role in maintaining the stability of up-methylated mRNAs in CHT-resident HSPCs. In addition, we analyzed the alternative splicing events between adjacent stages and identified very few alternative splicing events (Figure S1I), indicating that RNA splicing may not play crucial roles during HSPC development.

Here, we demonstrate that the dynamics of mRNA m⁵C modification accompany HSPC development. Analytic insights suggest that during the transition from AGM-derived HSPCs to CHT-resident HSPCs, m⁵C modification might be involved in the regulation of mRNA stability.

***Ybx1* is required for HSPC expansion**

To determine the functional involvement of mRNA m⁵C modification in HSPC development, we first examined mRNA expression of the key regulators of m⁵C by quantitative polymerase chain reaction (qPCR) with sorted *runx1*⁺ HSPCs, including methyltransferases (*nsun2* and *nsun6*) and binding proteins (*alyref* and *ybx1*). Notably, *ybx1* exhibited a comparatively higher expression level in HSPCs (Figure S2A), prompting us to further validate its expression pattern. Double fluorescence *in situ* hybridization (dFISH) and qPCR confirmed that *ybx1* was highly expressed in *cmyb*⁺ HSPCs in the CHT region at 36 hpf and *runx1*⁺ HSPCs at 60 hpf (Figures 2A and 2B). Considering that the role of mRNA m⁵C modification is mediated by its reader proteins,^{15,16} we focused on Ybx1 to examine the functional role of m⁵C modification in hematopoiesis.

To assess whether Ybx1 is required for HSPC development, we employed a knockdown approach using *ybx1* morpholino (MO), which resulted in a notable decrease in Ybx1 protein levels (Figure S2B). Whole-mount *in situ* hybridization (WISH) revealed that while HSPC generation (marked by *cmyb* at 33 hpf) remained relatively unaffected, the expression of HSPC marker *cmyb* was decreased in the CHT from 52 hpf and thereafter in

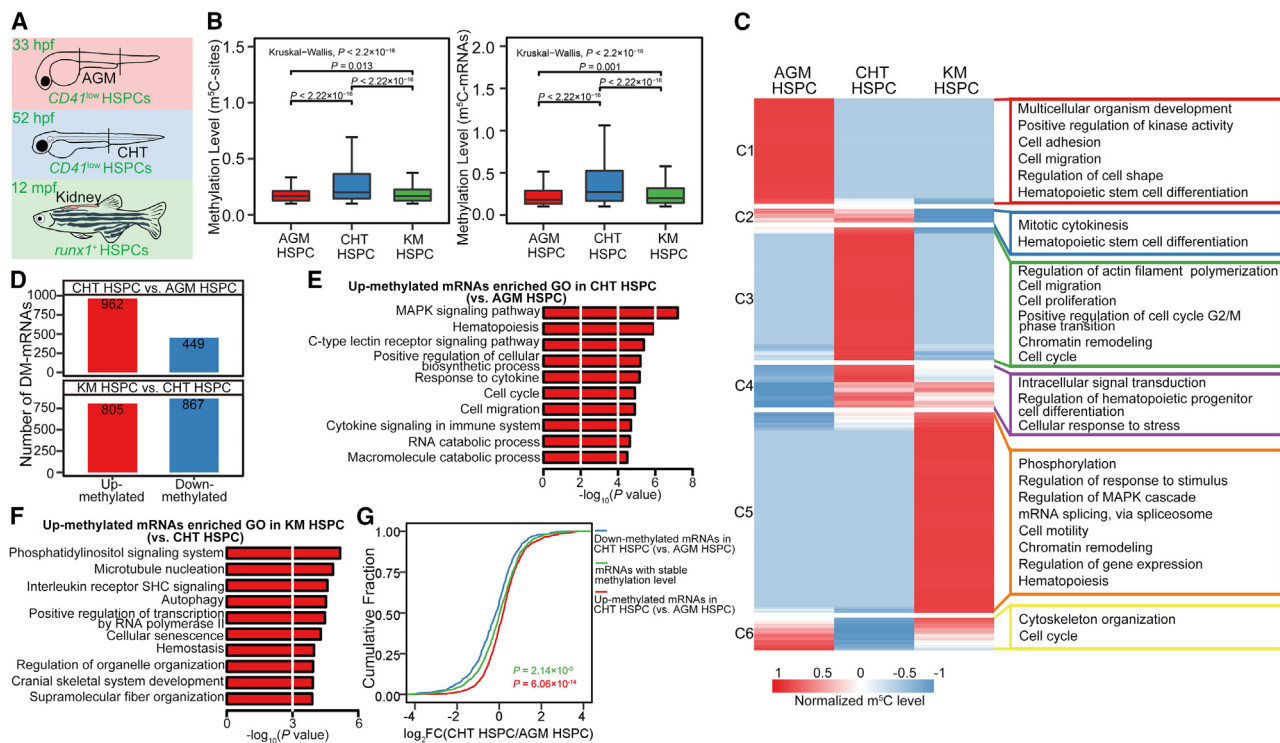


Figure 1. Dynamic transcriptomic landscapes of $m^5\text{C}$ modification during HSPC development

(A) Diagram of sorting HSPCs ($\text{CD}41\text{-GFP}^{\text{low}}$) at 33 hpf in the AGM region, at 52 hpf in the CHT region and HSPCs ($\text{runx1}\text{-enGFP}^+$), and at 12 mpf in the KM for RNA-BisSeq and RNA-seq. $n = 2$ biological replicates.

(B) Boxplots showing the methylation level of $m^5\text{C}$ sites (left) and $m^5\text{C}$ -modified mRNAs (right) in AGM-derived HSPCs, CHT-resident HSPCs, and KM-colonized HSPCs. The p values were determined using the Wilcoxon test and the Kruskal-Wallis test.

(C) Heatmap showing the dynamic methylated mRNAs in AGM-derived HSPCs, CHT-resident HSPCs and KM-colonized HSPCs, and corresponding GO biological processes for cluster-specific $m^5\text{C}$ -modified mRNAs. $m^5\text{C}$ level was normalized by Z score. C1–C6, Clusters 1–6. Clustering was performed with the default method.

(D) Bar charts showing the number of differentially methylated mRNAs between adjacent developmental stages.

(E and F) GO analysis of mRNAs with up-methylated levels in CHT-resident HSPCs compared to AGM-derived HSPCs (E) and in KM-colonized HSPCs compared to CHT-resident HSPCs (F).

(G) Cumulative distribution displaying the expression level changes of mRNAs with different methylation level between AGM-derived and CHT-resident HSPCs. The p value was calculated using the Wilcoxon test.

See also Figure S1.

ybx1 morphants (Figure S2C). Furthermore, live imaging showed that *ybx1* deficiency led to a decreased number of *runx1*:enGFP⁺ cells at 52 hpf, and then even more significant after 60 hpf (Figures S2D and S2E), validating the HSPC defects upon *ybx1* knockdown. In addition, we utilized previously reported *ybx1* mutants to confirm the *ybx1* loss-of-function phenotypes.²⁷ The zygotic mutants were obtained by cross-mating the *ybx1*^{+/−} adult fish; however, we failed to obtain the maternal-zygotic *ybx1* mutant embryos because of severe germ cell defects in adult female mutants and gastrulation arrest in embryos.^{22,27} Notably, the mutants had relatively unaltered HSPCs in comparison with siblings based on the results of WISH (expression of *cmyb* and *ikaros*), qPCR, and confocal imaging at 60 hpf (Figures 2C–2E), which were inconsistent with the HSPC phenotype in *ybx1* morphants. Previous studies have shown that maternal effects in zygotic mutants may alleviate phenotypic manifestations²⁸; consequently, suppressing this maternal effect through low-dose MO injection results in a more pronounced phenotype. Because of

the still-retained *ybx1* expression at 52 hpf (Figure S2F), we wondered whether the maternal effect may result in the alleviative phenotype in *ybx1* zygotic mutants. To assess this hypothesis, we injected low-dose (LD)-*ybx1* MO into siblings and *ybx1* zygotic mutants and observed that *ybx1* protein was cleared in *ybx1* mutants injected with LD-*ybx1* MO, but not in siblings (Figure S2F). WISH and qPCR results showed that *ybx1* mutants injected with LD *ybx1* MO exhibited the impaired HSPCs, which was similar to that in the *ybx1* morphants, but siblings injected with LD *ybx1* MO remained unaffected (Figures 2C and 2D). Confocal imaging confirmed a significant decrease of HSPCs in the CHT following *ybx1* deficiency (Figure 2E). Meanwhile, HSPC production remained unaffected (Figure S2G), which was consistent with that in *ybx1* morphants. Moreover, wild-type *ybx1* (*ybx1*^{WT}) mRNA and transcriptional activity-deficient *ybx1* (*ybx1* deleting nuclear localization signal [*ybx1*^{del NLS}]) mRNA^{29,30} could efficiently restore the decrease of HSPCs after *ybx1* depletion (Figures S2H–S2K), indicating that the defective

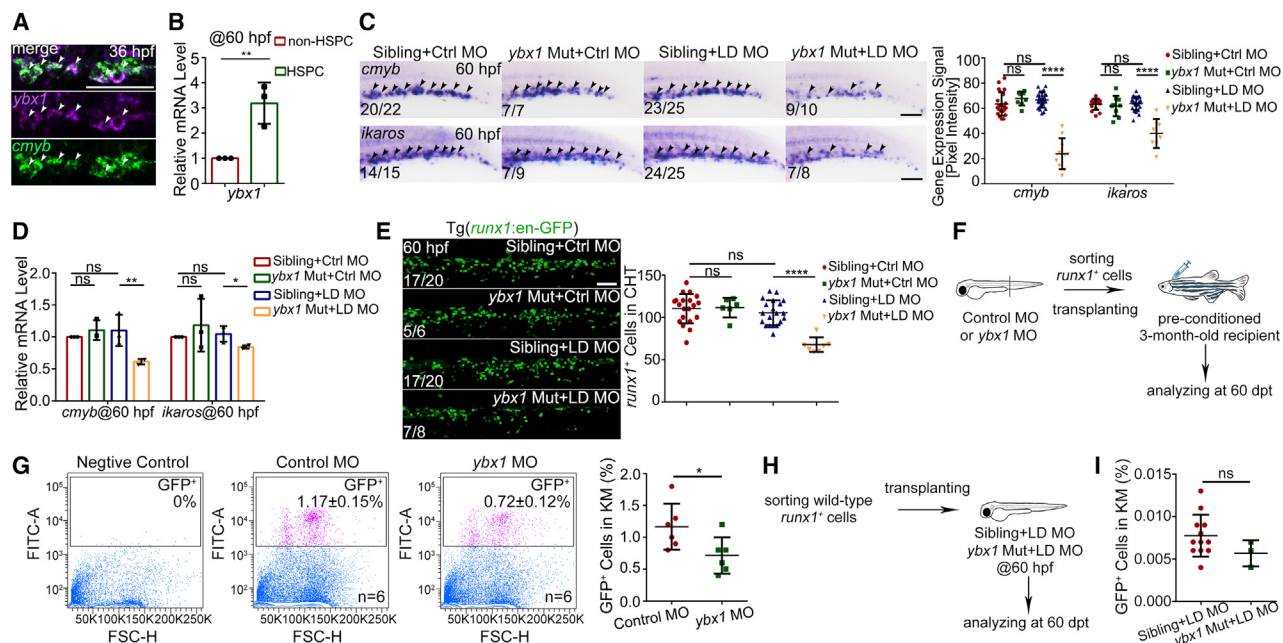


Figure 2. Ybx1 is cell autonomously required for HSPC expansion

(A) Double FISH showing the co-expression between *ybx1* and *cmyb* in HSPCs in the CHT region at 36 hpf. White arrowheads indicating the co-expressed cells. $n \geq 3$ biological replicates.

(B) Relative mRNA expression of *ybx1* in HSPCs (*runx1⁺*) and non-HSPCs (*runx1⁻*) at 60 hpf. $n = 3$ biological replicates.

(C and D) WISH (C) and qPCR with sorted *runx1⁺* HSPCs (D) examining *cmyb* and *ikaros* expression in control MO-injected sibling and *ybx1* mutant and low-dose (LD) *ybx1* MO-injected sibling and *ybx1* mutant in the CHT region at 60 hpf. The arrowheads indicate the expression of HSPC markers *cmyb* and *ikaros* (C). $n \geq 3$ biological replicates.

(E) Confocal imaging and statistical analysis (right) showing the *runx1⁺* HSPCs in the CHT region of control MO-injected sibling and *ybx1* mutant and LD *ybx1* MO-injected sibling and *ybx1* mutant at 60 hpf. $n \geq 3$ biological replicates.

(F) Experimental procedure of HSPC transplantation in irradiated-adult recipients.

(G) Flow cytometric and statistical analysis (right) of engrafted *runx1:en-GFP⁺* cells in the recipient KM at 60 dpt. WT Tubingen zebrafish whole KM cells as a negative control to gate *runx1:en-GFP⁺* HSPCs. n (control MO HSPCs > irradiated WT) = 6 recipients, n (*ybx1* MO HSPCs > irradiated WT) = 6 recipients.

(H) Experimental procedure of HSPC transplantation in zebrafish embryos.

(I) Flow cytometric statistical analysis of engrafted *runx1:en-GFP⁺* cells in the recipient KM at 60 dpt. n (*runx1⁺* HSPCs > Sibling + LD MO) = 12 recipients, n (*runx1⁺* HSPCs > *ybx1* Mut + LD MO) = 3 recipients.

Error bars, mean \pm SD. Two-tailed unpaired Student's t test; ns, no significance; * $p < 0.05$; ** $p < 0.01$; *** $p < 0.0001$ (B–D, E, G, and I). The numbers indicating the number of embryos with representative phenotype/total number of embryos in each group (C and E). Scale bars, 50 μ m (A and E) and 100 μ m (C).

See also Figure S2.

phenotype arose from the loss of function of *ybx1*, independent of its transcriptional activity.

Collectively, our findings demonstrate the essential role of *ybx1* in CHT-resident HSPC development.

Ybx1 regulates HSPC development in an HSPC-autonomous manner

To determine whether the HSPC defects in *ybx1*-deficient embryos is cell autonomous, we conducted transplantation experiments. An equal number of *runx1:en-GFP⁺* HSPCs isolated from control-MO and *ybx1* MO-injected embryos at 5 days postfertilization (dpf) were transplanted into irradiated adult recipients (Figure 2F). The *runx1:en-GFP⁺* cells were detectable in the tail region at 4 h posttransplantation (hpt) (Figure S2L). Flow cytometry analysis of the GFP⁺ cells in the KM at 60 days posttransplantation (dpt) revealed that the percentage of GFP⁺ cells derived from *ybx1* morphants was lower than that in control groups (Figure 2G). The multilineage analyses showed that the

progenitors and myeloid lineage reconstitution efficiency of *ybx1*-deficient HSPCs were decreased, while the erythroid lineage reconstitution efficiency was increased (Figure S2M). These results suggest that the impaired HSPCs in *ybx1*-deficient embryos are primarily due to intrinsic defects within the HSPCs. Additionally, we generated parabiotic embryo pairs with WT and *ybx1*-deficient embryos in Tg(*runx1:en-GFP*) or non-transgenic background (Figure S2N). The number of *runx1⁺* cells in the WT recipient CHT was significantly lower when *ybx1*-deficient embryos were used as donors than when WT were used (Figure S2O), indicating an HSPC cell-intrinsic defect after *ybx1* deficiency. In contrast, the number of WT *runx1⁺* HSPCs in *ybx1*-deficient recipient CHT was comparable to that in the WT recipient CHT (Figure S2O), suggesting that the CHT niche in *ybx1*-deficient embryos can support normal HSPC development.

To further verify whether the HSPC defects upon *ybx1* deficiency were due to the environmental factors, we sorted an equal

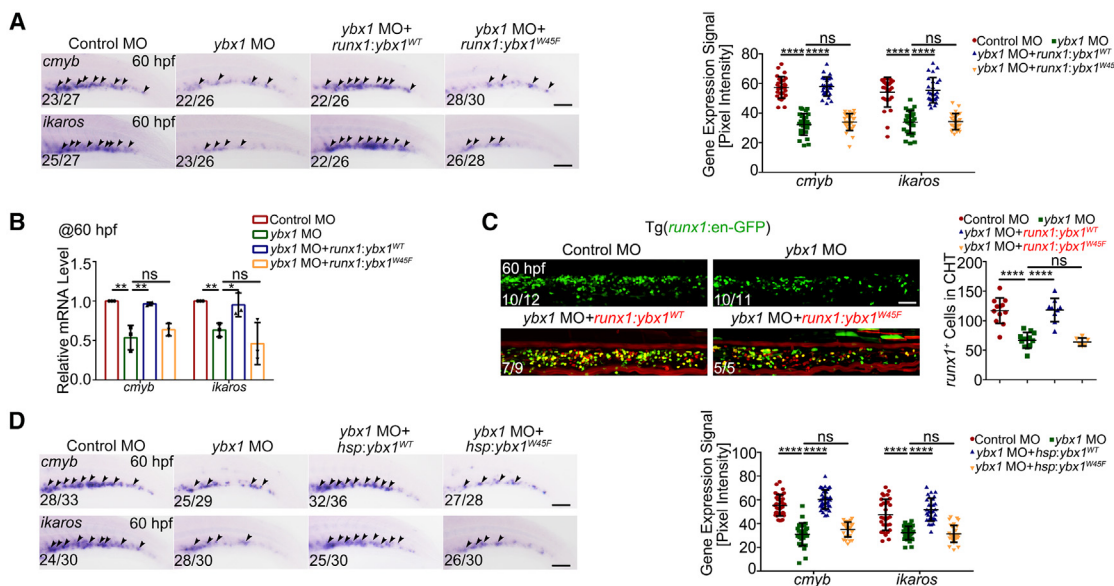


Figure 3. Ybx1 regulates HSPC expansion dependent on m^5C modification

(A and B) WISH results (A) and qPCR with sorted *runx1:en-GFP*⁺ cells (B) showing *cmyb* and *ikaros* expression in control morphants, *ybx1* morphants, Tg(*runx1:ybx1*^{WT}-tdTomato) embryos injected with *ybx1* MO, and Tg(*runx1:ybx1*^{W45F}-tdTomato) embryos injected with *ybx1* MO at 60 hpf in the CHT region. The arrowheads indicate the expression of *cmyb* or *ikaros*. (A). $n \geq 3$ biological replicates.

(C) Confocal imaging and statistical analysis (right) showing the *runx1:en-GFP*⁺ cells in the CHT region of control morphants, *ybx1* morphants, Tg(*runx1:ybx1*^{WT}-tdTomato) embryos injected with *ybx1* MO, and Tg(*runx1:ybx1*^{W45F}-tdTomato) embryos injected with *ybx1* MO at 60 hpf. $n \geq 3$ biological replicates.

(D) WISH results and statistical analysis (right) showing *cmyb* and *ikaros* expression in control morphants, *ybx1* morphants, Tg(*hsp70:ybx1*^{WT}-EGFP) embryos injected with *ybx1* MO, and Tg(*hsp70:ybx1*^{W45F}-EGFP) embryos injected with *ybx1* MO at 60 hpf in the CHT region. The arrowheads indicate the expression of *cmyb* or *ikaros*. $n \geq 3$ biological replicates.

Error bars, mean \pm SD. Two-tailed unpaired Student's t test; ns, no significance; * $p < 0.05$; ** $p < 0.01$; *** $p < 0.0001$ (A–D). The numbers indicating the number of embryos with representative phenotype/total number of embryos in each group (A, C, and D). Scale bars, 100 μ m (A and D) and 50 μ m (C).

See also Figure S3.

number of WT *runx1:en-GFP*⁺ HSPCs at 60 hpf and transplanted them into LD-MO-injected sibling and *ybx1* mutant embryonic recipients (Figure 2H). After 60 dpt, flow cytometry analysis showed that there was no significant difference in the percentage of *runx1:en-GFP*⁺ cells in the KM between sibling or *ybx1* mutant recipients (Figure 2I), suggesting an intact niche in the *ybx1* mutant. Moreover, the transplanted WT *runx1:en-GFP*⁺ HSPCs remained comparable in both WT and *ybx1* MO recipients at 48 hpt (Figure S2P), further indicating the CHT niche is unaffected by *ybx1* deficiency.

Furthermore, to investigate the direct role of *ybx1* in HSPCs, we performed HSPC-specific *ybx1*^{WT} overexpression driven by the *runx1* enhancer and the minimal promoter of β -globin (to ensure minimal activity)^{31,32} and confirmed the tdTomato fluorescence in *runx1:en-GFP*⁺ HSPCs (Figure S3A). WISH and qPCR showed that overexpression of *ybx1*^{WT} within HSPCs efficiently rescued the decreased expression of HSPC markers after *ybx1* deficiency (Figures 3A and 3B). Meanwhile, live imaging analysis further revealed that the reduced HSPC number in *ybx1* morphants could be restored by HSPC-specific *ybx1*^{WT} induction (Figure 3C), indicating the HSPC specific function of *ybx1*.

Taken together, these results demonstrate that Ybx1 is cell autonomously essential for HSPC development.

Ybx1 regulates HSPC expansion via m^5C recognition

Considering the m^5C binding activity of Ybx1, we next asked whether and how its recognition of m^5C contributed to fetal HSPC development. To address this issue, we generated a Ybx1 mutant form (*Ybx1*^{W45F}) featuring an amino acid substitution at the critical site for m^5C recognition (Figure S3B).^{21,22,33} We applied heat shock-inducible overexpression of *ybx1*^{WT} or *ybx1*^{W45F} and detected expression of EGFP and FLAG after heat shock (Figure S3C). Rescue experiments demonstrated that *ybx1*^{WT}, but not *ybx1*^{W45F}, significantly restored *cmyb* and *ikaros* expression in *ybx1*-deficient embryos (Figure 3D). In addition, the induction of *ybx1*^{W45F} within HSPCs was also unable to rescue the hematopoietic defects observed in *ybx1*-deficient embryos (Figures 3A–3C), suggesting that HSPC defects are specific to Ybx1 incompetence of binding to m^5C sites within HSPCs. Furthermore, to assess the potential of RNA m^5C modification in HSPC expansion, we treated zebrafish embryos with eltrombopag, which has been reported to bind to the TET2 catalytic domain and inhibit its dioxygenase activity.³⁴ TETs could catalyze the formation of 5-hydroxymethylcytidine in RNA.^{17,35} Eltrombopag treatment resulted in an increased mRNA m^5C level and a higher number of CHT-resident HSPCs (Figures S3D–S3F), indicating a correlation between elevated RNA m^5C level and HSPC expansion in the CHT.

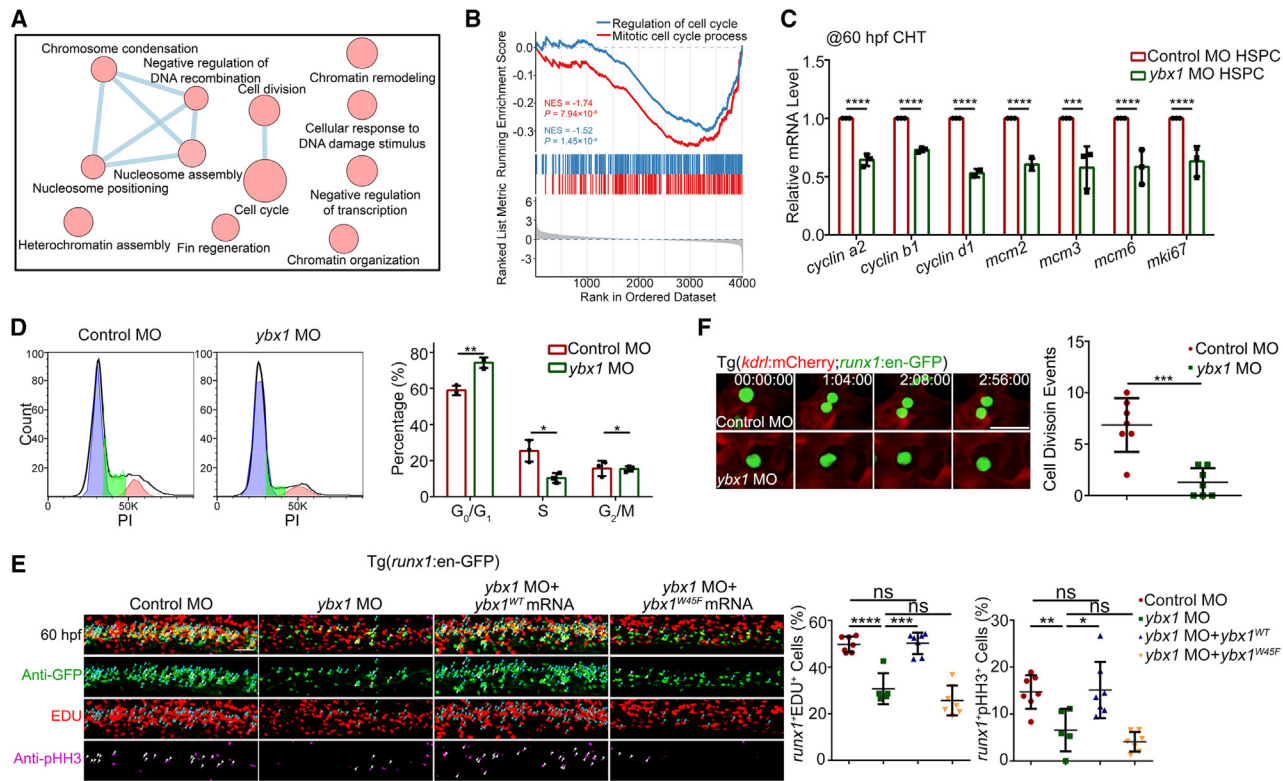


Figure 4. *ybx1* depletion leads to cell-cycle defects in HSPC

- (A) Function network of down-regulated Ybx1 binding mRNAs upon *ybx1* deficiency.
 - (B) GSEA showing the down-regulation of cell-cycle-related pathways upon *ybx1* deficiency, with the analysis focusing exclusively on mRNAs targeted by Ybx1.
 - (C) qPCR analysis showing the relative mRNA expression of Ybx1 binding targets in *runx1*⁺ HSPCs from control morphants and *ybx1* morphants at 60 hpf. *n* = 3 biological replicates.
 - (D) Flow cytometry and statistical analysis (right) of PI stained *runx1*⁺ cells from control morphants and *ybx1* morphants at 60 hpf. The y axis indicates cell number and the x axis indicates DNA content. *n* = 3 biological replicates.
 - (E) EdU and pHH3 staining and statistical analysis (right) in control morphants, *ybx1* morphants, embryos co-injected with *ybx1* MO, and *ybx1*^{WT} mRNA or *ybx1*^{W45F} mRNA at 60 hpf in the CHT region. Blue arrowheads indicate the EdU⁺*runx1*⁺ cells. White arrowheads indicate the pHH3⁺*runx1*⁺ cells. *n* = 3 biological replicates.
 - (F) Time-lapse confocal imaging of control morphants and *ybx1* morphants with Tg(*kdr*:mCherry; *runx1*:en-GFP) background. Right: statistical analysis of the cell division events of *runx1*:en-GFP⁺ cells. *n* (control MO) = 7 embryos, *n* (*ybx1* MO) = 7 embryos.
- Error bars, mean ± SD. Two-tailed unpaired Student's t test; ns, no significance; **p* < 0.05; ***p* < 0.01; ****p* < 0.001; *****p* < 0.0001 (C–F). Scale bars, 50 μm (E) and 25 μm (F).

See also Figure S4.

These results suggest that Ybx1-mediated m⁵C modification is required for CHT-resident HSPC expansion.

ybx1 depletion leads to cell-cycle defects in HSPCs

To further investigate the molecular mechanisms of Ybx1 in HSPC development, RNA-seq (using sorted CD41^{low} HSPCs from *ybx1*-deficient embryos at 52 hpf) (Figures S4A and S4B) and RNA immunoprecipitation sequencing (RIP-seq) for Ybx1 were performed (Figures S4C and S4D). We then combined RIP-seq with RNA-seq to identify differentially expressed Ybx1 binding targets in *ybx1*-deficient HSPCs.

The majority of Ybx1 binding peaks were located within the CDS regions (Figure S4E), consistent with the previous study.²²

Among 598 Ybx1 binding targets, the potential functions of the down-regulated 198 transcripts upon *ybx1* deficiency were associated with cell cycle, chromatin remodeling, and others

(Figure 4A). Gene set enrichment analysis (GSEA) was performed to interpret differential regulatory pathways of Ybx1-binding mRNAs upon *ybx1* deficiency. Mitotic cell cycle processes and regulation of cell-cycle-associated functions were down-regulated upon *ybx1* deficiency (Figure 4B). In total, we screened out 642 cell-cycle-related mRNAs expressed in CHT-resident HSPCs, 109 of these mRNAs were significantly down-regulated in *ybx1*-deficient HSPCs, while only 17 were up-regulated (Figure S4F). Then, we confirmed the downregulation of top candidate Ybx1-binding cell-cycle transcripts, such as *cyclins*, *mcm*s, and *mki67*, in *ybx1*-deficient CHT-resident HSPCs (Figure 4C), while these genes were not altered significantly in AGM-derived HSPCs (Figure S4G).

To determine whether the cell-cycle progression and proliferation in *ybx1*-deficient HSPCs were affected, propidium iodide (PI) staining with sorted *runx1*⁺ HSPCs were performed.

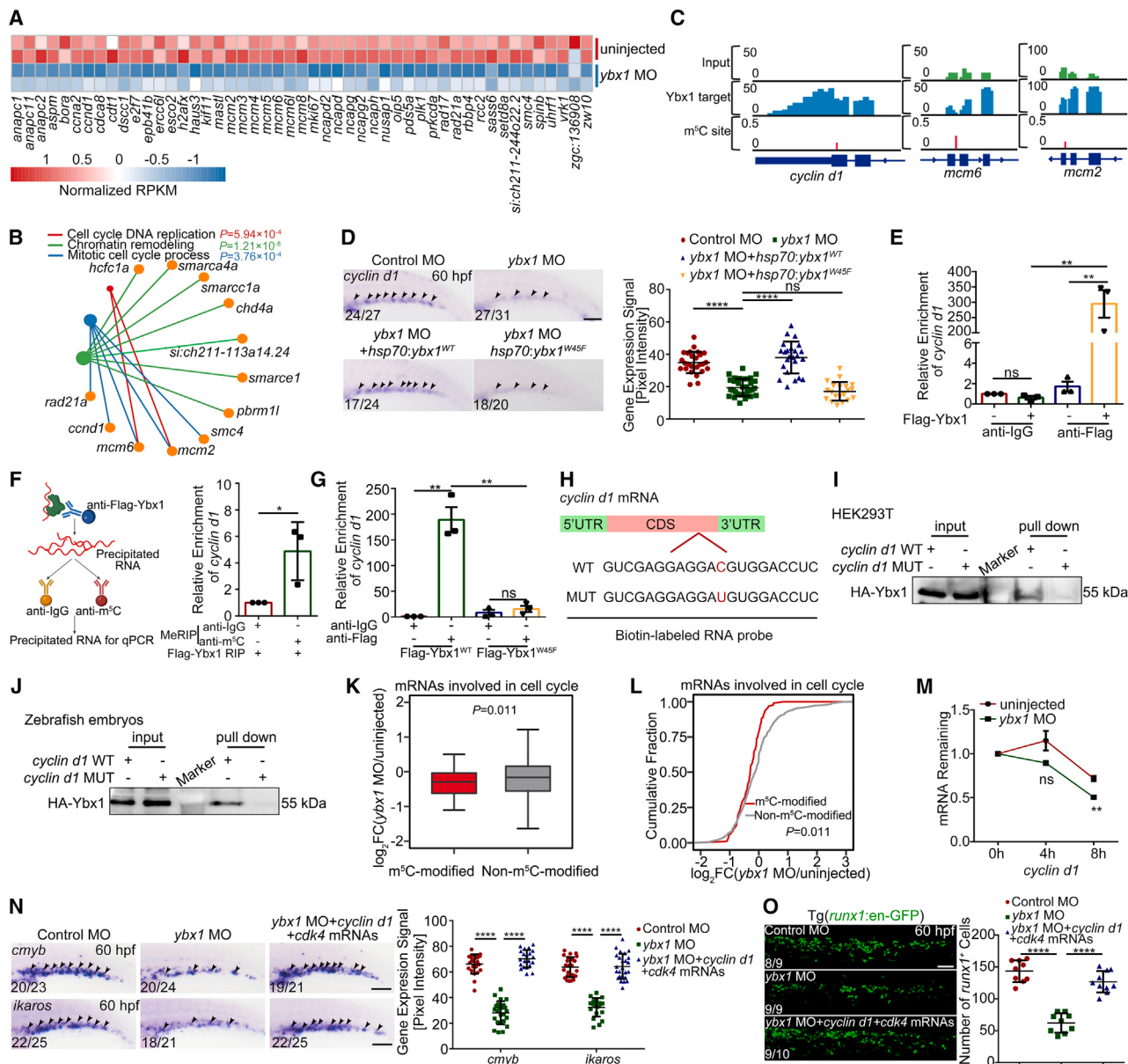


Figure 5. Ybx1 directly binds to and stabilizes cell-cycle transcripts deposited with m^5C .

- (A) Heatmap showing the expression of m^5C -modified mRNAs that were targeted by Ybx1 in uninjected and *ybx1* MO samples.
- (B) GO enrichment showing the down-regulated m^5C -modified mRNAs that were targeted by Ybx1 in *ybx1* morphants involved in the cell-cycle-associated functions.
- (C) IGV tracks displaying Ybx1 binding peaks (light blue shading) and m^5C sites (red line) distribution in *cyclin d1*, *mcm6*, and *mcm2*.
- (D) WISH results and statistical analysis (right) showing *cyclin d1* expression in control morphants, *ybx1* morphants, *Tg(hsp70:ybx1^{WT}-EGFP)*, or *Tg(hsp70:ybx1^{W45F}-EGFP)* embryos injected with *ybx1* MO at 60 hpf. The arrowheads indicate the expression of *cyclin d1*. $n \geq 3$ biological replicates.
- (E) RIP-qPCR analysis showing relative mRNA enrichment of *cyclin d1* in anti-immunoglobulin G (IgG) and anti-FLAG groups. $n = 3$ biological replicates.
- (F) Left: schematic illustration of using FLAG-Ybx1 precipitated RNA for m^5C methylated RNA immunoprecipitation-qPCR analysis. Right: qPCR analysis demonstrating the relative enrichment of *cyclin d1* in the anti- m^5C group compared to the anti-IgG control group, using RNAs precipitated by FLAG-Ybx1. $n = 3$ biological replicates.
- (G) RIP-qPCR analysis showing relative mRNA enrichment of *cyclin d1* in anti-IgG, anti-FLAG-Ybx1^{WT}, and anti-FLAG-Ybx1^{W45F} groups. $n = 3$ biological replicates.
- (H) Biotin-labeled RNA probes for both WT *cyclin d1* and its m^5C site synonymous mutant (MUT). The MUT nucleotide is highlighted in red.
- (I and J) Western blot showing HA-Ybx1 protein pulled down by biotin-labeled *cyclin d1* WT or MUT RNA probe. Pull-down assay in HEK293T cells (I) and in zebrafish embryos (J). $n = 3$ biological replicates.

(legend continued on next page)

Loss of *ybx1* led to an increased percentage of cells in G₀ and G₁ phases and a reduced proportion in S and G₂/M phases (**Figure 4D**). In addition, 5-ethynyl-2'-deoxyuridine (EdU) incorporation assay combined with immunostaining of phosphorylated histone H3 (pHH3) showed that the percentage of EdU⁺ *runx1*⁺ HSPCs (labeling S phase) and pHH3⁺ *runx1*⁺ HSPCs (labeling G₂/M phase) within CHT region began to decrease at 48 hpf in *ybx1*-deficient embryos and became more significant thereafter at 52 and 60 hpf (**Figures 4E, S4H**, and **S4I**), while the proportion within the AGM region was unchanged at 33 hpf (**Figure S4J**). These results suggest that Ybx1 targets cell-cycle-related transcripts and regulates cell-cycle progression of CHT-resident HSPCs. Moreover, *ybx1*^{WT} mRNA compared to *ybx1*^{W45F} mRNA was found to effectively rescue the decreased percentage of EdU⁺ *runx1*⁺ HSPCs and pHH3⁺ *runx1*⁺ HSPCs (**Figure 4E**), underscoring the importance of m⁵C binding capacity of Ybx1 in regulating the cell cycle in HSPCs. Subsequently, the time-lapse images revealed that *runx1*⁺ HSPCs in the CHT vascular niche divided frequently in the control morphants but hardly proliferated in the *ybx1* morphants (**Figures 4F, Videos S1 and S2**), implying impaired cell proliferation in CHT-resident HSPCs of *ybx1*-deficient embryos.

Next, to examine the survival status of HSPCs within the CHT region upon *ybx1* knockdown, TUNEL signal, *p53* and *p21* staining, and phosphorylated (Ser139) H2A.X protein level were examined (**Figures S4K–S4M**). The results showed that there was no apparent cell apoptosis and DNA damage after *ybx1* deficiency.

Overall, these findings demonstrate that Ybx1 targets cell-cycle-related transcripts and *ybx1* depletion leads to the arrest of HSPCs in the G₀ and G₁ phases. The reduced cell-cycle activity, but not apoptosis, ultimately contributes to the impaired HSPC expansion upon *ybx1* deficiency.

Ybx1 directly binds to and stabilizes cell-cycle transcripts deposited with m⁵C

To further explore the regulatory function of Ybx1 in regard to m⁵C, we integrated Ybx1 RIP-seq and RNA-BisSeq data (collected at 52 hpf) and found that there was a significant overlap between m⁵C-modified mRNAs and Ybx1-binding mRNAs (**Figure S5A**). Moreover, the distribution of Ybx1 binding peaks displayed a pattern similar to that of m⁵C peaks in the CDS region (**Figure S5B**), and showed a closer spatial proximity to these m⁵C peaks (**Figure S5C**), which suggests that m⁵C-modified mRNAs tend to be bound by Ybx1. For the down-regulated

m⁵C-modified Ybx1 targets upon *ybx1* deficiency (**Figure 5A**), we observed an enrichment of cell-cycle-related terms and mRNAs (**Figure 5B**) and the Integrative Genomics Viewer (IGV) tracks showed the m⁵C modification sites and the enrichment of Ybx1 binding regions on these mRNAs, including *cyclin d1*, *mcm6*, and *mcm2* (**Figure 5C**). WISH revealed a decreased expression of *cyclin d1* and *mcm6* in the CHT region after *ybx1* knockdown, which can be rescued by *ybx1*^{WT} mRNA overexpression, but not *ybx1*^{W45F} (**Figures 5D, S5D**, and **S5E**). FLAG-Ybx1 RIP-qPCR confirmed the interaction between *cyclin d1* and Ybx1 as well as *mcm6* and Ybx1 (**Figures 5E** and **S5F**).

To detect whether Ybx1 directly binds to m⁵C-modified cell-cycle transcripts, we initiated the FLAG-Ybx1 immunoprecipitation, followed by m⁵C immunoprecipitation utilizing the RNA product obtained from the Ybx1 RIP. Subsequently, we performed qPCR for the target transcripts (**Figure 5F**). The qPCR results showed a significantly higher enrichment of both *cyclin d1* and *mcm6* in the m⁵C immunoprecipitation group (**Figures 5F** and **S5G**). Additionally, the reduced enrichment by FLAG-Ybx1^{W45F} compared to FLAG-Ybx1^{WT} verified that Ybx1 bound to these transcripts (*cyclin d1* and *mcm6*) via recognizing m⁵C modification (**Figures 5G** and **S5H**). Furthermore, we performed RNA pull-down assays to further validate the recognition of m⁵C by Ybx1. We synthesized biotin-labeled WT and m⁵C site-synonymous mutant (MUT) *cyclin d1* RNA probes (**Figure 5H**) and found that HA-Ybx1 was much more pulled down by WT *cyclin d1* than that by MUT *cyclin d1* in both HEK293T cells and zebrafish embryos (**Figures 5I** and **5J**), and HA-Ybx1^{W45F} showed obvious less binding affinity to *cyclin d1* RNA (**Figure S5I**). The results above confirm the direct binding of Ybx1 to m⁵C-modified *cyclin d1* and *mcm6* mRNAs.

We then sought to determine how Ybx1 regulates cell-cycle transcripts. The expression abundance analysis showed that in embryos lacking *ybx1*, the abundance alterations were significantly more pronounced for mRNAs involved in the cell cycle that were modified by m⁵C, compared to those without m⁵C (**Figures 5K** and **5L**), suggesting that Ybx1 may regulate the stability of these m⁵C modified transcripts, which is consistent with the major role of m⁵C in mediating mRNA stability. To explore this possibility, we measured the mRNA levels of *cyclin d1* and *mcm6* following treatment with the RNA polymerase II inhibitor α-amanitin to inhibit transcription.^{36,37} Our results indicated that loss of *ybx1* led to a significant decrease in the levels of remaining *cyclin d1* and *mcm6* mRNAs (**Figures 5M** and **S5J**). Next, we synthesized m⁵C reporter mRNAs, where *cyclin d1* or *mcm6* with (WT) or without (MUT) an m⁵C site was fused to an EGFP tag

(K) Boxplot showing the overall expression-level change of m⁵C-modified and -unmodified mRNAs involved in the cell cycle after *ybx1* knockdown. The expression level was log₂ transformed. The significance was performed by the Wilcoxon test.

(L) Cumulative distribution displaying the expression-level change of m⁵C-modified and -unmodified mRNAs involving in the cell cycle. The significance was performed by the Wilcoxon test.

(M) qPCR analysis of the *cyclin d1* mRNA level at 0, 4, and 8 h after α-amanitin treatment in uninjected embryos and *ybx1* morphants. n = 3 biological replicates.

(N) WISH results and statistical analysis (right) showing *cmyb* and *ikaros* expression in control morphants, *ybx1* morphants, and embryos co-injected with *ybx1* MO, *cyclin d1*, and *cdk4* mRNAs at 60 hpf. The arrowheads indicate the expression of *cmyb* or *ikaros*. n ≥ 3 biological replicates.

(O) Confocal imaging and statistical analysis (right) showing *runx1*⁺ cells in control morphants, *ybx1* morphants, and embryos co-injected with *ybx1* MO, *cyclin d1*, and *cdk4* mRNAs at 60 hpf. n ≥ 3 biological replicates.

Error bars, mean ± SD. Two-tailed unpaired Student's t test; ns, no significance; *p < 0.05; **p < 0.01; ***p < 0.0001 (D–O). The numbers indicating the number of embryos with representative phenotype/total number of embryos in each group (D, N, and O). Scale bars, 100 μm (D and N) and 50 μm (O).

See also [Figure S5](#).

(Figure S5K). Upon *ybx1* depletion, WT *cyclin d1* or *mcm6* mRNA was diminished significantly compared to that in control embryos, reflected by EGFP fluorescence intensity and transcript level (Figures S5L–S5O). On the contrary, the MUT *cyclin d1* or *mcm6* was not altered in *ybx1*-deficient embryos (Figures S5P–S5S). These results demonstrate that the stability of m⁵C-modified *cyclin d1* and *mcm6* is positively regulated by Ybx1.

Furthermore, we showed that the cell-cycle progression of HSPCs was restored upon *cyclin d1-cdk4* (*cyclin-dependent kinase 4*) complex overexpression, as previously described,³⁸ which led to the reduced G₀/G₁ phase population and increased S phase population in HSPCs (Figures S5T–S5U), thereby mitigating the hematopoietic defects after *ybx1* deficiency (Figures 5N and 5O).

Ybx1 deletion results in the decay of m⁵C-modified cell-cycle-related mRNAs that typically function to disrupt the cell cycle, suggesting a plausible mechanism by which *ybx1*-deficient HSPCs display impaired proliferation.

***Ybx1* cooperates with *Pabpc1a* to regulate HSPC expansion**

It has been reported that the stability of m⁵C-modified mRNAs regulated by Ybx1 relies on the interacting partner Pabpc1a, which acts as an mRNA stabilizer by blocking deadenylation and endonucleolytic cleavage.^{22,39} Therefore, we asked whether Pabpc1a interacts with Ybx1 in facilitating m⁵C-modified mRNAs stabilization in HSPCs. Co-immunoprecipitation verified the direct interaction between FLAG-Pabpc1a and endogenous Ybx1 (Figure S6A). Moreover, similar to *ybx1*, *pabpc1a* was highly expressed in *runx1*⁺ HSPCs (Figure S6B), and immunofluorescence combined with dFISH revealed the co-localization of *pabpc1a* and *ybx1* in *cmyb*:EGFP HSPCs (Figure S6C), suggesting a collaborative function between Pabpc1a and Ybx1 in facilitating HSPC development.

To further explore the function of *pabpc1a* in HSPC development, we employed an MO knockdown approach and verified its efficiency (Figure S6D). Consistent with the defects observed after *ybx1* deficiency, the loss of *pabpc1a* led to significantly reduced expression of *cmyb* and *ikaros* in HSPCs (Figure S6E), indicating the crucial role of *pabpc1a* in CHT-resident HSPC development.

To investigate the underlying molecular mechanism, FLAG-Pabpc1a RIP-qPCR was performed, and the results confirmed the binding of Pabpc1a to m⁵C-modified Ybx1 targets *cyclin d1* and *mcm6* (Figures S6F and S6G). Similar to *ybx1* deficiency, loss of *pabpc1a* led to the decreased expression of both *cyclin d1* and *mcm6* in HSPCs (Figure S6H). The decreased percentage of BrdU⁺*cmyb*⁺ cells verified that the depletion of *pabpc1a* disturbed the cell cycle of HSPCs (Figure S6I). These results demonstrate that Ybx1 cooperates with Pabpc1a to stabilize m⁵C-modified cell-cycle-related mRNAs in HSPCs, thereby ensuring HSPC proliferation.

***Ybx1* is required for mouse FL HSPC expansion**

To determine whether the regulatory function of Ybx1 is conserved in mammal FL HSPCs, we examined Ybx1 expression in mouse FL at embryonic day 14.5 (E14.5) and

found the co-localization of Ybx1 with HSPC marker c-Kit (Figure 6A).

Subsequently, we knocked down endogenous *Ybx1* expression in mouse E14.5 FL lineage[−]Sca-1⁺c-Kit⁺ (LSK) cells using *Ybx1* small interfering RNAs (siRNAs) (Figures 6B, S6J, and S6K). Loss of *Ybx1* resulted in a significantly decreased proportion of LSK cells (Figures 6C and 6D). Moreover, the colony-forming units in culture assay showed that the colony-forming ability of LSK cells was significantly impaired after *Ybx1* deficiency (Figure 6E), indicating *Ybx1* is required for the function of mouse FL HSPCs. Correspondingly, the key hematopoietic-related genes were significantly down-regulated after *Ybx1* knockdown (Figure 6F). Loss of *Ybx1* caused the evidently decreased proportion of Ki67⁺ LSK cells and led to the down-regulated expression of cell-cycle-related genes (Figures 6G and S6L), implying a disrupted cell-cycle progression. Moreover, consistent with *ybx1*-deficient zebrafish embryos, the mRNA expression level of *Cyclin D1* and *Mcm6* declined due to strengthened mRNA decay upon *Ybx1* depletion in mouse FL HSPCs (Figure 6H). Collectively, our results support a conserved role of *Ybx1* in vertebrate HSPC development.

DISCUSSION

In this study, we have presented a comprehensive view of how dynamic RNA m⁵C landscape shapes HSPC expansion. Specifically, within expanding HSPCs (zebrafish CHT-resident HSPCs and mouse FL HSPCs), Ybx1 recognizes and stabilizes m⁵C-modified mRNAs associated with the cell cycle, collaborating with Pabpc1a.

The generation of nascent HSPC from AGM undergoes a process of EHT, during which the endothelial cells change cell morphology, down-regulate the expression of endothelial transcripts, and launch the hematopoietic program.^{40,41} Thereafter, HSPCs in mouse FL or zebrafish CHT are in an active cell-cycle state, expressing characteristic transcripts related to cell proliferation and biosynthetic process.^{42,43} Therefore, HSPC development involves dynamic transitions in the cell state, accompanied by shifts in the transcriptome to adapt to the requirement of the following developmental stage. However, the mechanism by which the output of transcripts is globally regulated timely for HSPC cell state transition remains poorly understood. Previous studies have focused mainly on developmental hematopoiesis regulation at the transcriptional level, such as chromatin accessibility, DNA methylation and histone modification.^{44–50} In the present study, we underscore the molecular mechanism of RNA m⁵C modification in regulating HSPC cell state transition by fine-tuning gene expression at the post-transcriptional level. We comprehensively profiled the landscape of RNA m⁵C modification during HSPC development and found that RNA m⁵C modification displays potential stage-specific functions. For example, in AGM-derived HSPCs, m⁵C modifies key transcripts related to HSPC budding and migration. In CHT-resident HSPCs, m⁵C turns to modify mRNAs of mitogen-activated protein kinase (MAPK) signaling pathway and cell-cycle processes, essential for HSPC proliferation. Furthermore, our study points out the molecular mechanism of RNA m⁵C in specific developmental stage of hematopoiesis, where the expression of

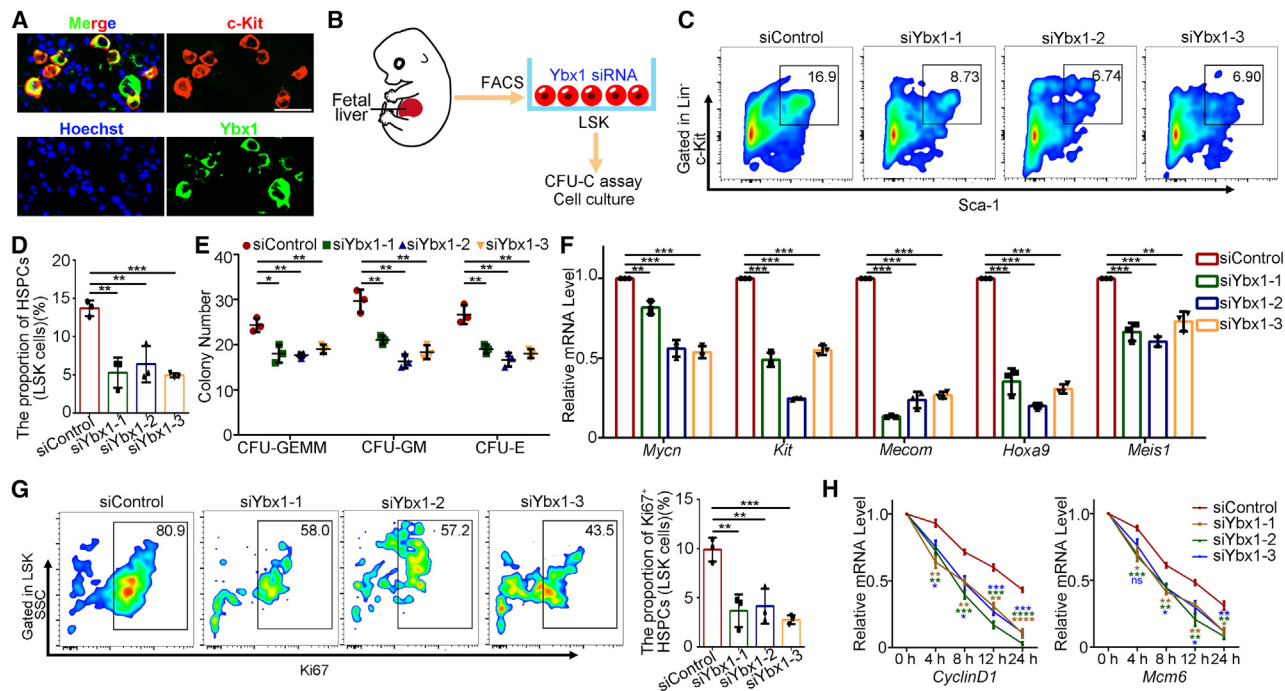


Figure 6. *Ybx1* is required for mouse fetal liver HSPC expansion

- (A) Immunofluorescence analysis of mouse *Ybx1* and c-Kit expression in E14.5 fetal liver (FL). $n = 3$ biological replicates.
 - (B) Workflow of knockdown of *Ybx1* in sorted mouse FL lineage⁻sca1⁺c-Kit⁺ (LSK) HSPCs and ex vivo HSPC culture.
 - (C) Flow cytometry analysis of HSPC proportion in control and *Ybx1* knockdown groups. $n = 3$ biological replicates.
 - (D) Statistical analysis of (C).
 - (E) Colony numbers of cultured HSPCs in control and *Ybx1* knockdown groups. $n = 3$ biological replicates.
 - (F) qPCR analysis showing the mRNA level of *Mycn*, *Kit*, *Mecom*, *Hoxa9*, and *Meis1* in control and *Ybx1* knockdown HSPCs. $n = 3$ biological replicates.
 - (G) Flow cytometry analysis and statistical analysis (right) of Ki67⁺ HSPC proportion in control and *Ybx1* knockdown groups. $n = 3$ biological replicates.
 - (H) qPCR analysis showing the *Cyclin D1* and *Mcm6* mRNA level at 0, 4, 8, 12, and 24 h after α -amanitin treatment in control and *Ybx1* knockdown HSPCs. $n = 3$ biological replicates.
- Error bars, mean \pm SD. Two-tailed unpaired Student's t test; * $p < 0.05$; ** $p < 0.01$; *** $p < 0.001$; **** $p < 0.0001$ (D–H). Scale bar, 25 μ m (A). CFU-E, CFU-erythroid; CFU-GEMM, CFU-granulocyte, erythrocyte, macrophage, megakaryocyte; CFU-GM, CFU-granulocyte, macrophage.

See also Figure S6.

cell-cycle-related transcripts is globally and tightly regulated by *Ybx1*-mediated RNA m⁵C during CHT-resident HSPC development.

Currently, although there have been several studies reporting the involvement of RNA m⁵C modifications in embryonic development, tumorigenesis, and rice adaptation to high temperature and others,^{17,21,22,33,51} our understanding of the biological function of RNA m⁵C modifications is relatively limited—in particular, its role and specific mechanisms in embryonic hematopoiesis. Here, we reveal the essential function of RNA m⁵C modification in the dynamic regulation of mRNA stability, which in turn shapes the epitranscriptomic reprogramming during the development from AGM-derived HSPCs to CHT-resident HSPCs. The consequence of the stabilized m⁵C-modified, cell-cycle-related mRNAs in HSPCs is to achieve an active cycling state, which could be applied to expand HSPCs. Notably, we discovered that treatment with a previously reported TET inhibitor significantly elevated the global mRNA m⁵C level and promoted HSPC expansion. However, the possibility of TET inhibitor treatment through its role on

DNA 5-methylcytosine is not excluded and awaits further investigation.

As a fundamental biological process, the cell cycle is predominantly organized by the core machinery components, such as cyclins and CDKs.^{52,53} The cyclin level oscillates during cell-cycle progression,^{54–56} which is regulated at both the transcriptional and posttranslational levels. For instance, *cyclin d1* transcription is governed by transcription factors and signaling pathways,⁵⁷ while posttranslational regulations, such as phosphorylation and ubiquitylation, modulate its protein level during the cell-cycle progression.^{55,56} Our study demonstrates that the stabilized m⁵C-modified mRNAs serve as a reliable source for timely protein synthesis when needed during the cell cycle, which emerges as an additional layer for the cell-cycle regulation at the posttranscriptional level. However, the mechanisms behind *Ybx1*-mediated m⁵C modification in achieving simultaneous regulation of multiple cell-cycle-related mRNAs remain unclear. It is noteworthy that both *Ybx1* and *Pabpc* have been reported to regulate biological processes by mediating liquid-liquid phase separation

(LLPS).^{58–61} Therefore, we hypothesize that in CHT-resident HSPCs, Ybx1 and Pabpc1a potentially mediate LLPS, enabling m⁵C-modified mRNAs (including cell-cycle-related mRNAs) to coexist in the liquid-like condensates for enhanced stabilization. However, whether LLPS contributes to the regulation of hematopoietic development through Ybx1-mediated m⁵C requires further investigation.

In summary, our study reveals that Ybx1-mediated stability of m⁵C-modified cell-cycle-related mRNAs is essential for HSPC expansion. This discovery provides new insights into our understanding of hematopoiesis at the epitranscriptomic level and holds potential for applications in expanding HSPCs *in vitro* through the modulation of mRNA modifications in the context of regenerative medicine.

Limitations of the study

It is important to note that m⁵C modifies a wide range of transcripts beyond cell-cycle-related mRNAs in the process of HSPC expansion. These include transcripts of hematopoietic transcription factors and those involved in the MAPK signaling pathway or cellular biosynthetic processes, which may also contribute to HSPC defects in *ybx1*-deficient embryos. A more comprehensive exploration of these aspects is expected in future studies. Furthermore, we cannot fully exclude the effect of TET inhibitor treatment on DNA m⁵C, but the increased level of RNA m⁵C methylation was indeed observed, suggesting its potential direct impact on RNA m⁵C modification. Further validation and mechanistic exploration are warranted to distinguish these possibilities.

RESOURCE AVAILABILITY

Lead contact

Further information and requests for resources and reagents should be directed to and will be fulfilled by the lead contact, Lu Wang (wanglu1@ihcams.ac.cn).

Materials availability

All plasmids and zebrafish transgenic lines generated by this study are available from the [lead contact](#) upon reasonable request.

Data and code availability

- The RNA-BisSeq, RNA-seq, and RIP-seq data reported in this paper have been deposited in the Genome Sequence Archive in the National Genomics Data Center, China National Center for Bioinformation/Beijing Institute of Genomics, Chinese Academy of Sciences. Original western blot images have been deposited at Mendeley Data. They are publicly available as of the date of publication. Accession numbers are listed in the [key resources table](#).
- All original code has been deposited at Zenodo and is publicly available as of the date of publication. The accession number is listed in the [key resources table](#).
- Any additional information required to reanalyze the data reported in this paper is available from the [lead contact](#) upon request.

ACKNOWLEDGMENTS

We thank Yifan Zhang for critical reading of the manuscript. This work was supported by grants from the National Natural Science Foundation of China (grant nos. 32222027, 92153303, and 92353000), the National Key Research and Development Program of China (grant no. 2018YFA0801200), the Tianjin Science Fund for Distinguished Young Scholars (grant no. 21JCJQJC00120),

the Youth Innovation Promotion Association of CAS (grant no. Y2022040), and the Postdoctoral Fellowship Program of CPSF (grant no. GZC20232569).

AUTHOR CONTRIBUTIONS

F.L. carried out the experiments, with assistance from G.S., Y.L., and P.S. M.W. and M.L. performed the bioinformatic analysis. S.G. validated the phenotype in mouse embryos. H.W. and W.L. helped to examine the mRNA m⁵C level. L.W., Y.Y., F.L., and Y.-G.Y. conceived the project, supervised the study, interpreted the data, and wrote the manuscript. All authors read and approved the final manuscript.

DECLARATION OF INTERESTS

The authors declare no competing interests.

STAR METHODS

Detailed methods are provided in the online version of this paper and include the following:

- **KEY RESOURCES TABLE**
- **EXPERIMENTAL MODEL AND STUDY PARTICIPANT DETAILS**
 - Zebrafish
 - Mouse
 - Cell line
- **METHOD DETAILS**
 - Morpholinos, mRNA, and plasmid construction
 - Whole-Mount *In situ* hybridization (WISH) and double-fluorescence *In situ* hybridization (FISH)
 - Quantitative Real-Time PCR (qPCR)
 - Western Blot
 - Zebrafish transplantation
 - Zebrafish parabiosis
 - Propidium iodide staining
 - Edu incorporation assay combined with immunostaining of pHH3
 - BrdU labeling
 - TUNEL assay
 - RNA immunoprecipitation sequencing (RIP-seq), RIP-qPCR and m⁵C RIP-qPCR
 - Pull-down assay
 - mRNA stability analysis
 - m⁵C reporter assay
 - Confocal microscopy
 - UHPLC-MS/MS analysis of m⁵C levels
 - Flow cytometry for mouse fetal liver cells
 - Small Interference RNA (siRNA) transfection
 - Colony-forming unit (CFU) assay
 - HSPC cell culture
 - Cell sorting, RNA preparation, and mRNA purification
 - RNA-seq and RNA-BisSeq library preparation
 - High-throughput sequencing data processing
 - Differential expressed gene (DEG) analysis
 - Dynamic changes of RNA m⁵C between adjacent stages
 - RNA abundance changes of m⁵C-modified mRNAs after *ybx1* deficiency
 - Distribution patterns analysis of Ybx1 targets and m⁵C peaks
 - Gene ontology (GO) analysis
 - Function network analysis
 - Gene Set Enrichment Analysis
- **QUANTIFICATION AND STATISTICAL ANALYSIS**

SUPPLEMENTAL INFORMATION

Supplemental information can be found online at <https://doi.org/10.1016/j.celrep.2025.115324>.

Received: December 22, 2023
 Revised: December 1, 2024
 Accepted: January 28, 2025
 Published: February 13, 2025

REFERENCES

- Laurenti, E., and Göttgens, B. (2018). From haematopoietic stem cells to complex differentiation landscapes. *Nature* 553, 418–426. <https://doi.org/10.1038/nature25022>.
- Zhang, Y., Gao, S., Xia, J., and Liu, F. (2018). Hematopoietic Hierarchy - An Updated Roadmap. *Trends Cell Biol.* 28, 976–986. <https://doi.org/10.1016/j.tcb.2018.06.001>.
- Bertrand, J.Y., Chi, N.C., Santoso, B., Teng, S., Stainier, D.Y.R., and Traver, D. (2010). Haematopoietic stem cells derive directly from aortic endothelium during development. *Nature* 464, 108–111. <https://doi.org/10.1038/nature08738>.
- Kissa, K., and Herbomel, P. (2010). Blood stem cells emerge from aortic endothelium by a novel type of cell transition. *Nature* 464, 112–115. <https://doi.org/10.1038/nature08761>.
- Boisset, J.C., van Cappellen, W., Andrieu-Soler, C., Galjart, N., Dzierzak, E., and Robin, C. (2010). In vivo imaging of haematopoietic cells emerging from the mouse aortic endothelium. *Nature* 464, 116–120. <https://doi.org/10.1038/nature08764>.
- Gao, S., Shi, Q., Zhang, Y., Liang, G., Kang, Z., Huang, B., Ma, D., Wang, L., Jiao, J., Fang, X., et al. (2022). Identification of HSC/MPP expansion units in fetal liver by single-cell spatiotemporal transcriptomics. *Cell Res.* 32, 38–53. <https://doi.org/10.1038/s41422-021-00540-7>.
- Murayama, E., Kissa, K., Zapata, A., Mordelet, E., Briolat, V., Lin, H.F., Handin, R.I., and Herbomel, P. (2006). Tracing hematopoietic precursor migration to successive hematopoietic organs during zebrafish development. *Immunity* 25, 963–975. <https://doi.org/10.1016/j.immuni.2006.10.015>.
- Xue, Y., Lv, J., Zhang, C., Wang, L., Ma, D., and Liu, F. (2017). The Vascular Niche Regulates Hematopoietic Stem and Progenitor Cell Lodgment and Expansion via Klf6a-ccl25b. *Dev. Cell* 42, 349–362.e4. <https://doi.org/10.1016/j.devcel.2017.07.012>.
- Song, H.D., Sun, X.J., Deng, M., Zhang, G.W., Zhou, Y., Wu, X.Y., Sheng, Y., Chen, Y., Ruan, Z., Jiang, C.L., et al. (2004). Hematopoietic gene expression profile in zebrafish kidney marrow. *Proc. Natl. Acad. Sci. USA* 101, 16240–16245. <https://doi.org/10.1073/pnas.0407241101>.
- Bennett, C.M., Kanki, J.P., Rhodes, J., Liu, T.X., Paw, B.H., Kieran, M.W., Langenau, D.M., Delahaye-Brown, A., Zon, L.I., Fleming, M.D., and Look, A.T. (2001). Myelopoiesis in the zebrafish, Danio rerio. *Blood* 98, 643–651. <https://doi.org/10.1182/blood.v98.3.643>.
- Zaccara, S., Ries, R.J., and Jaffrey, S.R. (2019). Reading, writing and erasing mRNA methylation. *Nat. Rev. Mol. Cell Biol.* 20, 608–624. <https://doi.org/10.1038/s41580-019-0168-5>.
- Shi, H., Wei, J., and He, C. (2019). Where, When, and How: Context-Dependent Functions of RNA Methylation Writers, Readers, and Erasers. *Mol. Cell* 74, 640–650. <https://doi.org/10.1016/j.molcel.2019.04.025>.
- Li, Z., Qian, P., Shao, W., Shi, H., He, X.C., Gogol, M., Yu, Z., Wang, Y., Qi, M., Zhu, Y., et al. (2018). Suppression of m6A reader Ythdf2 promotes hematopoietic stem cell expansion. *Cell Res.* 28, 904–917. <https://doi.org/10.1038/s41422-018-0072-0>.
- Xue, C., Chu, Q., Zheng, Q., Jiang, S., Bao, Z., Su, Y., Lu, J., and Li, L. (2022). Role of main RNA modifications in cancer: N6-methyladenosine, 5-methylcytosine, and pseudouridine. *Signal Transduct. Targeted Ther.* 7, 142. <https://doi.org/10.1038/s41392-022-01003-0>.
- Chen, Y.S., Yang, W.L., Zhao, Y.L., and Yang, Y.G. (2021). Dynamic transcriptomic m5C and its regulatory role in RNA processing. *Wiley Interdiscip. Rev. RNA* 12, e1639. <https://doi.org/10.1002/wrna.1639>.
- Gao, Y., and Fang, J. (2021). RNA 5-methylcytosine modification and its emerging role as an epitranscriptomic mark. *RNA Biol.* 18, 117–127. <https://doi.org/10.1080/15476286.2021.1950993>.
- Li, Y., Xue, M., Deng, X., Dong, L., Nguyen, L.X.T., Ren, L., Han, L., Li, C., Xue, J., Zhao, Z., et al. (2023). TET2-mediated mRNA demethylation regulates leukemia stem cell homing and self-renewal. *Cell Stem Cell* 30, 1072–1090.e10. <https://doi.org/10.1016/j.stem.2023.07.001>.
- Liu, J., Huang, T., Zhang, Y., Zhao, T., Zhao, X., Chen, W., and Zhang, R. (2021). Sequence-and structure-selective mRNA m5C methylation by NSUN6 in animals. *Natl. Sci. Rev.* 8, nwaa273. <https://doi.org/10.1093/nsr/nwaa273>.
- Yang, X., Yang, Y., Sun, B.F., Chen, Y.S., Xu, J.W., Lai, W.Y., Li, A., Wang, X., Bhattacharai, D.P., Xiao, W., et al. (2017). 5-methylcytosine promotes mRNA export—NSUN2 as the methyltransferase and ALYREF as an m5C reader. *Cell Res.* 27, 606–625. <https://doi.org/10.1038/cr.2017.55>.
- Zhang, C., Chen, Y., Sun, B., Wang, L., Yang, Y., Ma, D., Lv, J., Heng, J., Ding, Y., Xue, Y., et al. (2017). m6A modulates haematopoietic stem and progenitor cell specification. *Nature* 549, 273–276. <https://doi.org/10.1038/nature23883>.
- Chen, X., Li, A., Sun, B.F., Yang, Y., Han, Y.N., Yuan, X., Chen, R.X., Wei, W.S., Liu, Y., Gao, C.C., et al. (2019). 5-methylcytosine promotes pathogenesis of bladder cancer through stabilizing mRNAs. *Nat. Cell Biol.* 21, 978–990. <https://doi.org/10.1038/s41556-019-0361-y>.
- Yang, Y., Wang, L., Han, X., Yang, W.L., Zhang, M., Ma, H.L., Sun, B.F., Li, A., Xia, J., Chen, J., et al. (2019). RNA 5-Methylcytosine Facilitates the Maternal-to-Zygotic Transition by Preventing Maternal mRNA Decay. *Mol. Cell* 75, 1188–1202.e11. <https://doi.org/10.1016/j.molcel.2019.06.033>.
- Wang, M.K., Gao, C.C., and Yang, Y.G. (2023). Emerging Roles of RNA Methylation in Development. *Acc. Chem. Res.* 56, 3417–3427. <https://doi.org/10.1021/acs.accounts.3c00448>.
- Wang, Y., Wei, J., Feng, L., Li, O., Huang, L., Zhou, S., Xu, Y., An, K., Zhang, Y., Chen, R., et al. (2023). Aberrant m5C hypermethylation mediates intrinsic resistance to gefitinib through NSUN2/YBX1/QSOX1 axis in EGFR-mutant non-small-cell lung cancer. *Mol. Cancer* 22, 81. <https://doi.org/10.1186/s12943-023-01780-4>.
- Ma, H.L., Bizet, M., Soares Da Costa, C., Murisier, F., de Bony, E.J., Wang, M.K., Yoshimi, A., Lin, K.T., Riching, K.M., Wang, X., et al. (2023). SRSF2 plays an unexpected role as reader of m5C on mRNA, linking epitranscriptomics to cancer. *Mol. Cell* 83, 4239–4254.e10. <https://doi.org/10.1016/j.molcel.2023.11.003>.
- Wang, X., Wang, M., Dai, X., Han, X., Zhou, Y., Lai, W., Zhang, L., Yang, Y., Chen, Y., Wang, H., et al. (2022). RNA 5-methylcytosine regulates YBX2-dependent liquid-liquid phase separation. *Fundam. Res.* 2, 48–55. <https://doi.org/10.1016/j.fmre.2021.10.008>.
- Sun, J., Yan, L., Shen, W., and Meng, A. (2018). Maternal Ybx1 safeguards zebrafish oocyte maturation and maternal-to-zygotic transition by repressing global translation. *Development* 145, dev166587. <https://doi.org/10.1242/dev.166587>.
- Wang, L., Liu, Z., Lin, H., Ma, D., Tao, Q., and Liu, F. (2017). Epigenetic regulation of left-right asymmetry by DNA methylation. *EMBO J.* 36, 2987–2997. <https://doi.org/10.15252/embj.201796580>.
- Bates, M., Boland, A., McDermott, N., and Marignol, L. (2020). YB-1: The key to personalised prostate cancer management? *Cancer Lett.* 490, 66–75. <https://doi.org/10.1016/j.canlet.2020.07.006>.
- Mordovkina, D., Lyabin, D.N., Smolin, E.A., Sogorina, E.M., Ovchinnikov, L.P., and Eliseeva, I. (2020). Y-Box Binding Proteins in mRNP Assembly, Translation, and Stability Control. *Biomolecules* 10, 591. <https://doi.org/10.3390/biom10040591>.
- Ng, C.E.L., Yokomizo, T., Yamashita, N., Cirovic, B., Jin, H., Wen, Z., Ito, Y., and Osato, M. (2010). A Runx1 intronic enhancer marks hemogenic endothelial cells and hematopoietic stem cells. *Stem Cell.* 28, 1869–1881. <https://doi.org/10.1002/stem.507>.

32. Zhang, P., He, Q., Chen, D., Liu, W., Wang, L., Zhang, C., Ma, D., Li, W., Liu, B., and Liu, F. (2015). G protein-coupled receptor 183 facilitates endothelial-to-hematopoietic transition via Notch1 inhibition. *Cell Res.* 25, 1093–1107. <https://doi.org/10.1038/cr.2015.109>.
33. Zou, F., Tu, R., Duan, B., Yang, Z., Ping, Z., Song, X., Chen, S., Price, A., Li, H., Scott, A., et al. (2020). Drosophila YBX1 homolog YPS promotes ovarian germ line stem cell development by preferentially recognizing 5-methylcytosine RNAs. *Proc. Natl. Acad. Sci. USA* 117, 3603–3609. <https://doi.org/10.1073/pnas.1910862117>.
34. Guan, Y., Hasipek, M., Jiang, D., Tiwari, A.D., Grabowski, D.R., Pagliuca, S., Kongkiatkanon, S., Patel, B., Singh, S., Parker, Y., et al. (2022). Eltrombopag inhibits TET dioxygenase to contribute to hematopoietic stem cell expansion in aplastic anemia. *J. Clin. Investig.* 132, e149856. <https://doi.org/10.1172/jci149856>.
35. Fu, L., Guerrero, C.R., Zhong, N., Amato, N.J., Liu, Y., Liu, S., Cai, Q., Ji, D., Jin, S.G., Niedernhofer, L.J., et al. (2014). Tet-mediated formation of 5-hydroxymethylcytosine in RNA. *J. Am. Chem. Soc.* 136, 11582–11585. <https://doi.org/10.1021/ja505305z>.
36. Li, T., Gu, Y., Xu, B., Kuca, K., Zhang, J., and Wu, W. (2023). CircZBTB44 promotes renal carcinoma progression by stabilizing HK3 mRNA structure. *Mol. Cancer* 22, 77. <https://doi.org/10.1186/s12943-023-01771-5>.
37. Liu, Y., Li, C., Fang, L., Wang, L., Liu, H., Tian, H., Zheng, Y., Fan, T., and He, J. (2022). Lipid metabolism-related lncRNA SLC25A21-AS1 promotes the progression of oesophageal squamous cell carcinoma by regulating the NPM1/c-Myc axis and SLC25A21 expression. *Clin. Transl. Med.* 12, e944. <https://doi.org/10.1002/ctm2.944>.
38. Mende, N., Kuchen, E.E., Lesche, M., Grinenko, T., Kokkaliaris, K.D., Hennenberg, H., Lindemann, D., Dahl, A., Platz, A., Höfer, T., et al. (2015). CCND1-CDK4-mediated cell cycle progression provides a competitive advantage for human hematopoietic stem cells *in vivo*. *J. Exp. Med.* 212, 1171–1183. <https://doi.org/10.1084/jem.20150308>.
39. Grosset, C., Chen, C.Y., Xu, N., Sonenberg, N., Jacquemin-Sablon, H., and Shyu, A.B. (2000). A mechanism for translationally coupled mRNA turnover: interaction between the poly(A) tail and a c-fos RNA coding determinant via a protein complex. *Cell* 103, 29–40. [https://doi.org/10.1016/s0092-8674\(00\)00102-1](https://doi.org/10.1016/s0092-8674(00)00102-1).
40. Clements, W.K., and Traver, D. (2013). Signalling pathways that control vertebrate haematopoietic stem cell specification. *Nat. Rev. Immunol.* 13, 336–348. <https://doi.org/10.1038/nri3443>.
41. Wu, Y., and Hirschi, K.K. (2021). Regulation of Hemogenic Endothelial Cell Development and Function. *Annu. Rev. Physiol.* 83, 17–37. <https://doi.org/10.1146/annurev-physiol-021119-034352>.
42. Gao, S., and Liu, F. (2018). Fetal liver: an ideal niche for hematopoietic stem cell expansion. *Life Sci.* 61, 885–892. <https://doi.org/10.1007/s11427-018-9313-4>.
43. Xue, Y., Liu, D., Cui, G., Ding, Y., Ai, D., Gao, S., Zhang, Y., Suo, S., Wang, X., Lv, P., et al. (2019). A 3D Atlas of Hematopoietic Stem and Progenitor Cell Expansion by Multi-dimensional RNA-Seq Analysis. *Cell Rep.* 27, 1567–1578.e5. <https://doi.org/10.1016/j.celrep.2019.04.030>.
44. Ding, Y., Wang, W., Ma, D., Liang, G., Kang, Z., Xue, Y., Zhang, Y., Wang, L., Heng, J., Zhang, Y., and Liu, F. (2021). Smarca5-mediated epigenetic programming facilitates fetal HSPC development in vertebrates. *Blood* 137, 190–202. <https://doi.org/10.1182/blood.2020005219>.
45. Han, L., Madan, V., Mayakonda, A., Dakle, P., Woon, T.W., Shyamsunder, P., Nordin, H.B.M., Cao, Z., Sundaresan, J., Lei, I., et al. (2019). Chromatin remodeling mediated by ARID1A is indispensable for normal hematopoiesis in mice. *Leukemia* 33, 2291–2305. <https://doi.org/10.1038/s41375-019-0438-4>.
46. Xu, B., Cai, L., Butler, J.M., Chen, D., Lu, X., Allison, D.F., Lu, R., Rafii, S., Parker, J.S., Zheng, D., and Wang, G.G. (2018). The Chromatin Remodeler BPTF Activates a Stemness Gene-Expression Program Essential for the Maintenance of Adult Hematopoietic Stem Cells. *Stem Cell Rep.* 10, 675–683. <https://doi.org/10.1016/j.stemcr.2018.01.020>.
47. Petruk, S., Mariani, S.A., De Dominicis, M., Porazzi, P., Minieri, V., Cai, J., Iacovitti, L., Flomberg, N., Calabretta, B., and Mazo, A. (2017). Structure of Nascent Chromatin Is Essential for Hematopoietic Lineage Specification. *Cell Rep.* 19, 295–306. <https://doi.org/10.1016/j.celrep.2017.03.035>.
48. Bröske, A.M., Vockentanz, L., Kharazi, S., Huska, M.R., Mancini, E., Scheller, M., Kuhl, C., Enns, A., Prinz, M., Jaenisch, R., et al. (2009). DNA methylation protects hematopoietic stem cell multipotency from myeloerythroid restriction. *Nat. Genet.* 41, 1207–1215. <https://doi.org/10.1038/ng.463>.
49. Challen, G.A., Sun, D., Jeong, M., Luo, M., Jelinek, J., Berg, J.S., Bock, C., Vasantha Kumar, A., Gu, H., Xi, Y., et al. (2011). Dnmt3a is essential for hematopoietic stem cell differentiation. *Nat. Genet.* 44, 23–31. <https://doi.org/10.1038/ng.1009>.
50. Gao, P., Chen, C., Howell, E.D., Li, Y., Tober, J., Uzun, Y., He, B., Gao, L., Zhu, Q., Siekmann, A.F., et al. (2020). Transcriptional regulatory network controlling the ontogeny of hematopoietic stem cells. *Genes Dev.* 34, 950–964. <https://doi.org/10.1101/gad.338202.120>.
51. Tang, Y., Gao, C.C., Gao, Y., Yang, Y., Shi, B., Yu, J.L., Lyu, C., Sun, B.F., Wang, H.L., Xu, Y., et al. (2020). OsNSUN2-Mediated 5-Methylcytosine mRNA Modification Enhances Rice Adaptation to High Temperature. *Dev. Cell* 53, 272–286.e7. <https://doi.org/10.1016/j.devcel.2020.03.009>.
52. Malumbres, M., and Barbacid, M. (2009). Cell cycle, CDKs and cancer: a changing paradigm. *Nat. Rev. Cancer* 9, 153–166. <https://doi.org/10.1038/nrc2602>.
53. Suski, J.M., Braun, M., Strmiska, V., and Sicinski, P. (2021). Targeting cell-cycle machinery in cancer. *Cancer Cell* 39, 759–778. <https://doi.org/10.1016/j.ccr.2021.03.010>.
54. Baldin, V., Lukas, J., Marcote, M.J., Pagano, M., and Draetta, G. (1993). Cyclin D1 is a nuclear protein required for cell cycle progression in G1. *Genes Dev.* 7, 812–821. <https://doi.org/10.1101/gad.7.5.812>.
55. Fasanaro, P., Capogrossi, M.C., and Martelli, F. (2010). Regulation of the endothelial cell cycle by the ubiquitin-proteasome system. *Cardiovasc. Res.* 85, 272–280. <https://doi.org/10.1093/cvr/cvp244>.
56. Lin, D.I., Barbash, O., Kumar, K.G.S., Weber, J.D., Harper, J.W., Klein-Szanto, A.J.P., Rustgi, A., Fuchs, S.Y., and Diehl, J.A. (2006). Phosphorylation-dependent ubiquitination of cyclin D1 by the SCF(FBX4-alphaB crystallin) complex. *Mol. Cell* 24, 355–366. <https://doi.org/10.1016/j.molcel.2006.09.007>.
57. Klein, E.A., and Assoian, R.K. (2008). Transcriptional regulation of the cyclin D1 gene at a glance. *J. Cell Sci.* 121, 3853–3857. <https://doi.org/10.1242/jcs.039131>.
58. Liu, B., Shen, H., He, J., Jin, B., Tian, Y., Li, W., Hou, L., Zhao, W., Nan, J., Zhao, J., et al. (2023). Cytoskeleton remodeling mediated by circRNA-YBX1 phase separation suppresses the metastasis of liver cancer. *Proc. Natl. Acad. Sci. USA* 120, e2220296120. <https://doi.org/10.1073/pnas.2220296120>.
59. Heng, J., Shi, B., Zhou, J.Y., Zhang, Y., Ma, D., Yang, Y.G., and Liu, F. (2023). Cpeb1b-mediated cytoplasmic polyadenylation of shha mRNA modulates zebrafish definitive hematopoiesis. *Proc. Natl. Acad. Sci. USA* 120, e2212212120. <https://doi.org/10.1073/pnas.2212212120>.
60. Riback, J.A., Katanski, C.D., Kear-Scott, J.L., Pilipenko, E.V., Rojek, A.E., Sosnick, T.R., and Drummond, D.A. (2017). Stress-Triggered Phase Separation Is an Adaptive, Evolutionarily Tuned Response. *Cell* 168, 1028–1040.e19. <https://doi.org/10.1016/j.cell.2017.02.027>.
61. Liu, X., Wei, Q., Yang, C., Zhao, H., Xu, J., Mobet, Y., Luo, Q., Yang, D., Zuo, X., Chen, N., et al. (2024). RNA m5C modification upregulates E2F1 expression in a manner dependent on YBX1 phase separation and promotes tumor progression in ovarian cancer. *Exp. Mol. Med.* 56, 600–615. <https://doi.org/10.1038/s12276-024-01184-4>.
62. Lin, H.F., Traver, D., Zhu, H., Dooley, K., Paw, B.H., Zon, L.I., and Handin, R.I. (2005). Analysis of thrombocyte development in CD41-GFP transgenic zebrafish. *Blood* 106, 3803–3810. <https://doi.org/10.1182/blood-2005-01-0179>.

63. North, T.E., Goessling, W., Walkley, C.R., Lengerke, C., Kopani, K.R., Lord, A.M., Weber, G.J., Bowman, T.V., Jang, I.H., Grosser, T., et al. (2007). Prostaglandin E2 regulates vertebrate haematopoietic stem cell homeostasis. *Nature* 447, 1007–1011. <https://doi.org/10.1038/nature05883>.
64. Kimmel, C.B., Ballard, W.W., Kimmel, S.R., Ullmann, B., and Schilling, T.F. (1995). Stages of embryonic development of the zebrafish. *Dev. Dyn.* 203, 253–310. <https://doi.org/10.1002/aja.1002030302>.
65. Sorokin, A.V., Selyutina, A.A., Skabkin, M.A., Guryanov, S.G., Nazimov, I.V., Richard, C., Th'ng, J., Yau, J., Sorensen, P.H.B., Ovchinnikov, L.P., and Evdokimova, V. (2005). Proteasome-mediated cleavage of the Y-box-binding protein 1 is linked to DNA-damage stress response. *EMBO J.* 24, 3602–3612. <https://doi.org/10.1038/sj.emboj.7600830>.
66. Wang, L., Liu, T., Xu, L., Gao, Y., Wei, Y., Duan, C., Chen, G.Q., Lin, S., Patient, R., Zhang, B., et al. (2013). Fev regulates hematopoietic stem cell development via ERK signaling. *Blood* 122, 367–375. <https://doi.org/10.1182/blood-2012-10-462655>.
67. Wang, L., Zhang, P., Wei, Y., Gao, Y., Patient, R., and Liu, F. (2011). A blood flow-dependent klf2a-NO signaling cascade is required for stabilization of hematopoietic stem cell programming in zebrafish embryos. *Blood, The Journal of the American Society of Hematology* 118, 4102–4110.
68. He, J., Mo, D., Chen, J., and Luo, L. (2020). Combined whole-mount fluorescence *in situ* hybridization and antibody staining in zebrafish embryos and larvae. *Nat. Protoc.* 15, 3361–3379. <https://doi.org/10.1038/s41596-020-0376-7>.
69. Picelli, S., Faridani, O.R., Björklund, A.K., Winberg, G., Sagasser, S., and Sandberg, R. (2014). Full-length RNA-seq from single cells using Smart-seq2. *Nat. Protoc.* 9, 171–181. <https://doi.org/10.1038/nprot.2014.006>.
70. Zhang, C., Lv, J., He, Q., Wang, S., Gao, Y., Meng, A., Yang, X., and Liu, F. (2014). Inhibition of endothelial ERK signalling by Smad1/5 is essential for haematopoietic stem cell emergence. *Nat. Commun.* 5, 3431. <https://doi.org/10.1038/ncomms4431>.
71. Murayama, E., Sarris, M., Redd, M., Le Guyader, D., Vivier, C., Horsley, W., Trede, N., and Her bomel, P. (2015). NACA deficiency reveals the crucial role of somite-derived stromal cells in haematopoietic niche formation. *Nat. Commun.* 6, 8375. <https://doi.org/10.1038/ncomms9375>.
72. Tamplin, O.J., Durand, E.M., Carr, L.A., Childs, S.J., Hagedorn, E.J., Li, P., Yzaguirre, A.D., Speck, N.A., and Zon, L.I. (2015). Hematopoietic stem cell arrival triggers dynamic remodeling of the perivascular niche. *Cell* 160, 241–252. <https://doi.org/10.1016/j.cell.2014.12.032>.
73. Lv, P., and Liu, F. (2023). Heme-deficient primitive red blood cells induce HSPC ferroptosis by altering iron homeostasis during zebrafish embryogenesis. *Development* 150, dev201690. <https://doi.org/10.1242/dev.201690>.
74. Lv, P., Ma, D., Gao, S., Zhang, Y., Bae, Y.K., Liang, G., Gao, S., Choi, J.H., Kim, C.H., Wang, L., and Liu, F. (2020). Generation of foxn1/Casper Mutant Zebrafish for Allograft and Xenograft of Normal and Malignant Cells. *Stem Cell Rep.* 15, 749–760. <https://doi.org/10.1016/j.stemcr.2020.07.020>.
75. Hagedorn, E.J., Cillis, J.L., Curley, C.R., Patch, T.C., Li, B., Blaser, B.W., Riquelme, R., Zon, L.I., and Shah, D.I. (2016). Generation of Parabiotic Zebrafish Embryos by Surgical Fusion of Developing Blastulae. *J. Vis. Exp.* 112, 54168. <https://doi.org/10.3791/54168>.
76. Kiss, K., Murayama, E., Zapata, A., Cortés, A., Perret, E., Machu, C., and Her bomel, P. (2008). Live imaging of emerging hematopoietic stem cells and early thymus colonization. *Blood* 111, 1147–1156. <https://doi.org/10.1182/blood-2007-07-099499>.
77. Martin, M. (2011). Cutadapt removes adapter sequences from high-throughput sequencing reads. *EMBnet. journal* 17, 10–12. <https://doi.org/10.14806/ej.17.1.200>.
78. Bolger, A.M., Lohse, M., and Usadel, B. (2014). Trimmomatic: a flexible trimmer for Illumina sequence data. *Bioinformatics* 30, 2114–2120. <https://doi.org/10.1093/bioinformatics/btu170>.
79. Kim, D., Langmead, B., and Salzberg, S.L. (2015). HISAT: a fast spliced aligner with low memory requirements. *Nat. Methods* 12, 357–360. <https://doi.org/10.1038/nmeth.3317>.
80. Liao, Y., Smyth, G.K., and Shi, W. (2014). featureCounts: an efficient general purpose program for assigning sequence reads to genomic features. *Bioinformatics* 30, 923–930. <https://doi.org/10.1093/bioinformatics/btt656>.
81. Feng, J., Liu, T., Qin, B., Zhang, Y., and Liu, X.S. (2012). Identifying ChIP-seq enrichment using MACS. *Nat. Protoc.* 7, 1728–1740. <https://doi.org/10.1038/nprot.2012.101>.
82. Quinlan, A.R., and Hall, I.M. (2010). BEDTools: a flexible suite of utilities for comparing genomic features. *Bioinformatics* 26, 841–842. <https://doi.org/10.1093/bioinformatics/btq033>.
83. Rieder, D., Amort, T., Kugler, E., Lusser, A., and Trajanoski, Z. (2016). meRanTK: methylated RNA analysis ToolKit. *Bioinformatics* 32, 782–785. <https://doi.org/10.1093/bioinformatics/btv647>.
84. Robinson, M.D., McCarthy, D.J., and Smyth, G.K. (2010). edgeR: a Bioconductor package for differential expression analysis of digital gene expression data. *Bioinformatics* 26, 139–140. <https://doi.org/10.1093/bioinformatics/btp616>.
85. Dennis, G., Jr., Sherman, B.T., Hosack, D.A., Yang, J., Gao, W., Lane, H.C., and Lempicki, R.A. (2003). DAVID: Database for Annotation, Visualization, and Integrated Discovery. *Genome Biol.* 4, P3.
86. Shannon, P., Markiel, A., Ozier, O., Baliga, N.S., Wang, J.T., Ramage, D., Amin, N., Schwikowski, B., and Ideker, T. (2003). Cytoscape: a software environment for integrated models of biomolecular interaction networks. *Genome Res.* 13, 2498–2504. <https://doi.org/10.1101/gr.1239303>.
87. Yu, G., Wang, L.G., Han, Y., and He, Q.Y. (2012). clusterProfiler: an R package for comparing biological themes among gene clusters. *OMICS* 16, 284–287. <https://doi.org/10.1089/omi.2011.0118>.
88. Dobrzycki, T., Krencmarik, M., and Monteiro, R. (2020). Genotyping and Quantification of In Situ Hybridization Staining in Zebrafish. *J. Vis. Exp.* 10, e59956.

STAR★METHODS

KEY RESOURCES TABLE

REAGENT or RESOURCE	SOURCE	IDENTIFIER
Antibodies		
Anti-Digoxigenin-AP	Roche	Cat# 11093274910; RRID: AB_514497
Anti-Fluorescence-POD	Roche	Cat# 11426346910; RRID: AB_840257
Anti-Digoxigenin-POD	Roche	Cat# 11633716001; RRID: AB_514499
Anti-GFP	Thermo Fisher Scientific	Cat# A11122; RRID: AB_221569
Alexa Fluor 594 Goat Anti-Rabbit IgG (H + L) Antibody	Thermo Fisher Scientific	Cat# A11037; RRID: AB_2534095
Alexa Fluor 488 Goat Anti-Rabbit IgG (H + L) Antibody	Thermo Fisher Scientific	Cat# A11034; RRID: AB_2576217
Alexa Fluor 555 Goat Anti-Mouse IgG (H + L) Antibody	Thermo Fisher Scientific	Cat# A21422; RRID: AB_2535844
5-Methylcytosine Antibody	Active Motif	Cat# 39649; RRID: AB_2687950
Rabbit Polyclonal Anti-Ybx1 Antibody	Yang et al., ²² prepared by AbMax Biotechnology Co., Ltd	Cat# JYZ042-1
Rabbit Polyclonal Anti-PABP1 Antibody	Cell Signaling Technology	Cat# 4992; RRID: AB_10693595
Mouse Monoclonal Anti-Phospho-Histone H3 (Ser10) Antibody	Cell Signaling Technology	Cat# 9706; RRID: AB_331748
Rabbit Polyclonal Anti-β-Actin Antibody	Cell Signaling Technology	Cat# 4967S; RRID: AB_330288
Rabbit Polyclonal Anti-Flag Antibody	Sigma-Aldrich	Cat# F7425; RRID: AB_439687
Rabbit Monoclonal Anti-HA Antibody	Cell Signaling Technology	Cat# 3724S; RRID: AB_1549585
Rabbit Monoclonal Anti-Ybx1 Antibody	Abcam	Cat# Ab76149; RRID: AB_2219276
CD117 (c-Kit) Monoclonal Antibody (2B8), APC	Thermo Fisher Scientific	Cat# 17-1171-82; RRID: AB_469430
Ly-6A/E (Sca-1) Monoclonal Antibody (D7), PE-Cyanine7	Thermo Fisher Scientific	Cat# 25-5981-81; RRID: AB_469668
FITC Anti-mouse Lineage	BioLegend	Cat# 133302; RRID: AB_10697030
eFluor™ 450 Anti-mouse Ki-67	Thermo Fisher Scientific	Cat# 48-5698-80; RRID: AB_11151155
Rabbit monoclonal Anti-Histone H2A.XS139ph	GeneTex	Cat# GTX637288
Chemicals, peptides, and recombinant proteins		
DPBS	Gibco	Cat# C14190500BT
Fetal Bovine Serum	Sigma-Aldrich	Cat# F8687
Fetal Bovine Serum	Gibco	Cat# 16000044
1X RBC lysis buffer	eBioscience	Cat# 00-4333-57
MethoCult GF M3434	StemCell Technologies	Cat# 03434
Stemspam SFEM	StemCell Technologies	Cat# 09600
Recombinant murine SCF	PeproTech	Cat# 250-03
Recombinant murine IL6	PeproTech	Cat# 216-16
Recombinant murine TPO	PeproTech	Cat# 315-14
Recombinant murine Flt3-Ligand	PeproTech	Cat# 250-31L
2.5% Trypsin	Gibco	Cat# 15090046
UltraPure Glycogen	Invitrogen	Cat# 10814010
DIG RNA Labeling Mix	Roche	Cat# 11277073910
KAPA HiFi HotStart ReadyMix (2X)	Roche	Cat# KK2601
SuperScript II Reverse Transcriptase	Invitrogen	Cat# 18064-014
Betaine Solution	Sigma-Aldrich	Cat# B0300-1VL
Fluorescein RNA Labeling Mix	Roche	Cat# 11685619910
BM Purple	Roche	Cat# 11442074001
Blocking Reagent	Roche	Cat# 11096176001
TRNzol Reagent	TIANGEN	Cat# DP424
TRIzol Reagent	Invitrogen	Cat# 15596018
RNase Inhibitor	TaKaRa	Cat# 2313A

(Continued on next page)

Continued

REAGENT or RESOURCE	SOURCE	IDENTIFIER
RNase Inhibitor	TOYOBO	Cat# SIN-201
DNase I	NEBuilder	Cat# M0303S
HiFi DNA Assembly Master Mix	NEBuilder	Cat# E2621S
SuperReal PreMix Plus (SYBR Green)	TIANGEN	Cat# FP205
FxCycle PI/RNase	Invitrogen	Cat# F10797
DAPI	Sigma-Aldrich	Cat# D9542
Bovine Serum Albumin	Genview	Cat# 9048-46-8
Ribonuclease Inhibitor	Promega	Cat# N2515
Protease Inhibitor Cocktails	Roche	Cat# 11873580001
Anti-Flag M2 Affinity Gel	Sigma-Aldrich	Cat# A2220
Dynabeads Protein A	Invitrogen	Cat# 10001D
Dynabeads MyOne Streptavidin C1	Invitrogen	Cat# 65001
Bovine Serum Albumin	NEBuilder	Cat# B9001S
Proteinase K	Roche	Cat# 03115828001
VAHTS mRNA Capture Beads	Vazyme	Cat# N401
α -amanitin	MedChemExpress	Cat# HY-19610
NuPAGE™M 4–12% Bis-Tris Gel	Invitrogen	Cat# NP0335BOX
NuPAGE LDS Sample Buffer	Invitrogen	Cat# NP0007
NuPAGE™M MES SDS Running Buffer	Invitrogen	Cat# NP0002
RNeasy Mini Kit	QIAGEN	Cat# 74104
Immobilon Western Chemiluminescent	Millipore	Cat# WBKLS0500
HRP Substrate		
Lipofectamine™ RNAiMAX	Invitrogen	Cat# 13778030
HiScript III RT SuperMix for qPCR	Vazyme	Cat# R323-01
ChamQ Universal SYBR qPCR Master Mix	Vazyme	Cat# Q711-02
Fixation/Permeabilization Buffer	Invitrogen	Cat# 00-5523-00
Critical commercial assays		
mMessage mMachine SP6 kit	Invitrogen	Cat# AM1340
Moloney Murine Leukemia	Promega	Cat# M1708
Virus (M-MLV) Reverse Transcript		
<i>In Situ</i> Cell Death Detection Kit, TMR red	Roche	Cat# 12156792910
EdU Cell Proliferation Kit with Alexa Fluor 594	Beyotime	Cat# C0078S
RevertAid™ First Strand cDNA Synthesis kit	Invitrogen	Cat# K1622
VAHTS Universal V6 RNA-seq Library Prep Kit	Vazyme	Cat# NR604
TSA Cyanine 5	Akoya	Cat# NEL745001KT
TSA Fluorescein	Akoya	Cat# NEL741001KT
Fixation/Permeabilization Kit	BD Biosciences	Cat# 554714
KAPA Stranded mRNA-Seq Kit	KAPA	Cat# K8401
10 \times RNA Fragmentation Reagent	Ambion	Cat# AM8740
40% Sodium Bisulfite	Sigma-Aldrich	Cat# 243973-500G
3K Omega 500/pk Columns	PALL	Cat# OD003C35
RNase-free Tris-HCl Buffer (1 M, pH 9.0)	TIANDZ	Cat# 80933
PEI MAX (MW40,000)	Polysciences	Cat# 24765-100
7-AAD Viability Staining Solution	BioLegend	Cat# 420404
Deposited data		
RNA-Seq	This paper	GSA:CRA013943
RNA-BisSeq	This paper	GSA:CRA013943
Flag-Ybx1 RIP-Seq	This paper	GSA:CRA013943

(Continued on next page)

Continued

REAGENT or RESOURCE	SOURCE	IDENTIFIER
Original western blot images	This paper	Deposited at Mendeley at [https://doi.org/10.17632/np7267tp5w.1]
Experimental models: Cell lines		
Human: 293T	ATCC	CRL-11268; RRID: CVCL_1926
Experimental models: Organisms/strains		
Zebrafish: <i>CD41</i> :GFP	Lin et al. ⁶²	NA
Zebrafish: <i>runx1</i> :en-GFP	Zhang et al. ³²	NA
Zebrafish: <i>kdr1</i> :mCherry	Bertrand et al. ³	NA
Zebrafish: <i>cmyb</i> :EGFP	North et al. ⁶³	NA
Mouse: C57BL/6	SPF (Beijing) Biotechnology Co., Ltd.	NA
Oligonucleotides		
See Table S1 for list of primers	This paper	NA
<i>ybx1</i> MO: 5'- GTGGCTCTCTAGTGTTTCCC-3'	Yang et al. ²²	NA
Control MO: 5'-CCTCTTACCTCAGTTACAATTTATA-3'	This paper	NA
<i>pabpc1a</i> MO: 5'-TTCATTTCACGGCTGGAGGGTTT-3'	Yang et al. ²²	NA
see Table S1 for siRNA sequence for <i>ybx1</i> knockdown	This paper	NA
<i>cyclin d1</i> WT: GUCGAGGAGGACGUGGACCUC	This paper	NA
<i>cyclin d1</i> MUT: GUCGAGGAGGAUGUGGACCUC	This paper	NA
Recombinant DNA		
Plasmid: <i>hsp70</i> -flag- <i>ybx1</i> ^{WT} -EGFP	This paper	NA
Plasmid: <i>hsp70</i> -flag- <i>ybx1</i> ^{W45F} -EGFP	This paper	NA
Plasmid: pCS2+- <i>ybx1</i>	This paper	NA
Plasmid: pCS2+- <i>ybx1</i> ^{W45F}	This paper	NA
Plasmid: pCS2+- <i>ybx1</i> ^{del NLS}	This paper	NA
Plasmid: pCS2+-EGFP- <i>ybx1</i> ^{WT}	This paper	NA
Plasmid: pCS2+-EGFP- <i>ybx1</i> ^{del NLS}	This paper	NA
Plasmid: <i>runx1</i> -flag- <i>ybx1</i> ^{WT} -tdTomato	This paper	NA
Plasmid: <i>runx1</i> -flag- <i>ybx1</i> ^{W45F} -tdTomato	This paper	NA
Plasmid: pCS2+-HA- <i>ybx1</i>	This paper	NA
Plasmid: pCS2+-HA- <i>ybx1</i> ^{W45F}	This paper	NA
Plasmid: pCS2+-EGFP- <i>cyclin d1</i> -WT	This paper	NA
Plasmid: pCS2+-EGFP- <i>cyclin d1</i> -MUT	This paper	NA
Plasmid: pCS2+-EGFP- <i>mcm6</i> -WT	This paper	NA
Plasmid: pCS2+-EGFP- <i>mcm6</i> -MUT	This paper	NA
Plasmid: <i>hsp70</i> -flag- <i>pabpc1a</i> -EGFP	This paper	NA
Software and algorithms		
Data analysis	Graph Pad Prism 6	https://www.graphpad.com/
Imaging analysis	Photoshop CC2018	https://www.adobe.com/cn/
Imaging analysis	Bitplane Imaris 7.4.2	http://www.bitplane.com/
Imaging analysis	Imaris X64.9.3.1	http://www.bitplane.com/
Imaging analysis	ImageJ	https://imagej.nih.gov/ij/
Data analysis	Flowjo_V10	https://www.flowjo.com/
All original code	This paper	Deposited at Zenodo at [https://doi.org/10.5281/zenodo.14214768].

EXPERIMENTAL MODEL AND STUDY PARTICIPANT DETAILS

Zebrafish

Wild-type Tubingen and transgenic lines including *CD41*:GFP, *runx1*:en-GFP, *kdr1*:mCherry and *cmyb*:EGFP were raised in system water at 28.5°C. Zebrafish embryos were staged as described.⁶⁴ Embryos were used irrespective of their sex since zebrafish do not

display sexual dimorphism at larval stage. Adult HSPC samples were collected from pooled males and females that were randomly chosen. The zebrafish study was approved by the Ethical Review Committee of the State Key Laboratory of Experimental Hematology, National Clinical Research Center for Blood Diseases, Institute of Hematology & Blood Diseases Hospital, Chinese Academy of Medical Sciences & Peking Union Medical College, China.

Mouse

Wild type C57BL/6 were purchased from HFK (Beijing) Bioscience Co., Ltd and SPF (Beijing) Biotechnology Co., Ltd. The mice (8-10-week-old) of both sexes were used in equal proportions. The morning that the vaginal plug was detected is defined as embryonic day (E) 0 and the E14.5 fetal livers (FLs) were used for HSPC experiments. The present study was approved by the Ethics Committee for Animal Research of School of Life Sciences, Shandong University, China. All experimental assays with mice were performed in accordance with guidelines of the care and use of laboratory animals.

Cell line

The HEK293T cell line obtained from ATCC (RRID: CVCL_1926) was cultured in standard DMEM (Gibco) with 10% FBS (Sigma-Aldrich) and 1× penicillin/streptomycin (Invitrogen) in humidified 5% CO₂, 37°C incubators. The cell line was tested for mycoplasma contamination.

METHOD DETAILS

Morpholinos, mRNA, and plasmid construction

The antisense MOs (*ybx1* UTR MO, Control MO and *pabpc1a* ATG MO) were purchased from GeneTools. 1.5 ng *ybx1* MO, 1.5 ng Control MO and 0.5 ng *pabpc1a* MO were injected into 1~4-cell stage embryos. For low dose MO injection, 0.5 ng *ybx1* MO were used. *ybx1*^{del NLS} DNA sequences was constructed by deletion of the nuclear localization sequence (NLS) homologous to human.^{29,30,65} The mRNAs were synthesized using SP6 mMessage Machine kit and 100–200 pg of mRNA were injected into 1-cell stage embryos as previous study described.⁶⁶ The *ybx1*^{WT} and *ybx1*^{W45F} DNA sequences were cloned into pDestTol2pA2 plasmid containing *hsp70* promoter or *runx1* enhancer and fluorescent protein (EGFP or tdTomato) using HiFi DNA Assembly Master Mix (NEBuilder). 30 pg of *tol2* mRNA and 30 pg plasmid were injected into zebrafish embryos at 1-cell stage.

Whole-Mount *In situ* hybridization (WISH) and double-fluorescence *In situ* hybridization (FISH)

Zebrafish embryo WISH was performed using RNA probes of *cmyb*, *ikaros*, *cyclin d1*, *mcm6*, *p53* and *p21* as previously reported.^{20,67} Double-FISH was performed as previously reported⁶⁸ with *ybx1*, *pabpc1a*, and *cmyb* probes.

In brief, gene-specific PCR products were cloned to pGEM-T vector (Promega). After linearization, the probe was transcribed with DIG or fluorescein (Flu) labeling NTPs. For WISH, an RNA probe labeled by DIG was detected by AP-conjugated anti-DIG antibody (Roche). The BM purple (Roche) as substrate. For double-FISH, one probe was labeled by DIG and detected by POD-conjugated anti-DIG antibody, and the other was labeled by Flu and detected by POD-conjugated anti-fluorescein antibody. TSA Plus Cy5 solution, TSA Plus Cy3 solution and TSA Plus Fluorescein solution (Akoya) were used as substrates. For subsequent immunofluorescence, the embryos were incubated with anti-GFP antibody (Invitrogen) and following Alexa Fluor 488 Goat Anti-Rabbit IgG (H + L) antibody (Invitrogen).

Quantitative Real-Time PCR (qPCR)

1000 *runx1*⁺ cells sorted from 33hpf (AGM region), 60 hpf (CHT region) and 12mpf (kidney marrow) zebrafish were collected for total RNA extraction with TRIzol (Invitrogen). The RNA was reverse-transcribed and amplified as previously described.⁶⁹

Tissue (50% epiboly: whole embryo) of zebrafish embryos ($n = 30$) was extracted by TRNzol reagent (TIANGEN) and reversely transcribed by M-MLV Reverse Transcriptase (Promega).

The qPCR experiments were performed using SYBR Green (TIANGEN) on QuantStudio3 Real-Time PCR system (Thermo Fisher). Three independent experiments were performed in triplicate. Primer sequences used are presented in Table S1.

Western Blot

The protein was detected by following the previously described protocol.⁷⁰ In detail, zebrafish embryos were lysed, and protein was extracted using lysis buffer (50 mM Tris-HCl pH 7.4, 150 mM NaCl, 1 mM EDTA, 0.5 mM DTT, 0.5% NP-40, 0.2% SDS, 5%(v/v) Glycerol, cocktail protease inhibitor (Roche)). Samples were separated by SDS-PAGE and transferred to the PVDF membrane. Blocked with 5% BSA in 1×TBST for 1 h, the membrane was incubated with corresponding antibodies at 4°C overnight. The following antibodies were used: anti-β-Actin antibody (Cell Signaling Technology, 1:1000), anti-Ybx1 antibody (AbMax, 1:1000), anti-Flag antibody (Sigma-Aldrich, 1:1000), anti-HA antibody (Cell Signaling Technology, 1:1000), anti-Histone H2A.XS139ph antibody (GeneTex, 1:500), anti-Pabp antibody (Cell Signaling Technology, 1:1000) and anti-Ybx1 antibody (Abcam, 1:1000). Protein levels were visualized using West Pico PLUS Chemiluminescent Substrate (Invitrogen) by ChemiDoc (Bio-Rad).

Zebrafish transplantation

The transplantation assay in zebrafish embryonic recipient was performed as previously described.^{8,71} 2×10^5 *runx1*⁺ cells from wild type embryos at 55 hpf were sorted and resuspended with 4 µL PBS (containing 10% FBS). Using a microinjection apparatus, an equal number of donor cells were transplanted into the duct of cuvier of stage-matched recipient embryos. 1 nL contains about 50 cells. *runx1*⁺ cells were recorded by confocal microscope at 48 h post transplantation (hpt). The engraftment efficiency was assessed at 60 dpt by detecting the proportion of *runx1:en-GFP*⁺ cells in recipient KM using flow cytometry.

The transplantation assay in zebrafish irradiated adult recipient was performed as previously described.⁷²⁻⁷⁴ Recipient fish (3-month-old wild type Tubingen) were irradiated using 25 Gy. After 2 days, irradiated fish were used for transplantation. 4×10^5 *runx1*⁺ cells from both the tail region of control MO- and *ybx1* MO-injected embryos at 5 dpf were sorted and resuspended with 20 µL PBS (containing 1% FBS). The cells were injected into recipients using a 26s-gauge Hamilton 80,366 syringe by retroorbital injection. Each recipient fish was injected with 1 µL cell suspension, containing 2×10^4 *runx1*⁺ cells. The photographs of transplanted *runx1*⁺ cells were taken at 4 hpt in the tail region. The engraftment efficiency was assessed at 60 dpt by detecting the proportion of *runx1:en-GFP*⁺ cells in recipient KM using flow cytometry.

Zebrafish parabiosis

The wild-type and *ybx1*-deficient embryos in Tg(*runx1:en-GFP*) or non-transgenic background were fused at about 3 hpf and then developed into parabiotic embryo pairs as previously described.⁷⁵

Propidium iodide staining

The sorted *runx1*⁺ cells or *CD41*⁺ cells ($n = 2 \times 10^4$) were centrifuged and resuspended with 500 µL fixation and permeabilization buffer (BD) for 20 min at 4°C. After centrifuged, the pellet was washed with washing buffer (BD) twice and resuspended with 500 µL FxCycle PI/RNase Solution. Incubated for 15–30 min at room temperature in the dark, the stained cell suspension was detected by flow cytometry. Three independent experiments were performed.

EdU incorporation assay combined with immunostaining of pH3

The *runx1:en-GFP*⁺ embryos injected with EdU (10 mM) (Beyotime) were cultured at 28.5°C for 2 h and fixed in 4% paraformaldehyde (PFA). The fixed embryos were treated with Proteinase K (Vetec, 10 µg/mL) after rehydration and washed with PBST. The embryos were incubated with anti-phospho-Histone H3 (Ser10) antibody (mouse, Cell Signaling Technology, 1:500) and anti-GFP antibody (rabbit, Invitrogen, 1:1000) at 4°C overnight. Following washed with PBST, the embryos were treated with Alexa Fluor 555 Goat anti-mouse IgG (H + L) Antibody (1:800) and Alexa Fluor 488 Goat anti-rabbit IgG (H + L) Antibody (1:800). Incubated with EdU staining mix buffer (Beyotime) for 30 min at room temperature, the embryos were washed and mounted using 70% glycerol and pictures were taken by a confocal microscope. Three independent experiments were performed.

BrdU labeling

The *cmyb:EGFP*⁺ embryos injected with BrdU (10mM) (Roche) were cultured at 28.5°C for 2 h and fixed in 4% paraformaldehyde (PFA). The fixed embryos were treated with Proteinase K (Vetec, 10 µg/mL) after rehydration and washed with PBST. Following 2 mol/L HCl, the embryos were blocked and incubated with anti-BrdU solution (mouse, 1:800) and anti-GFP antibody (rabbit, Invitrogen, 1:1000) at 4°C overnight. Following washing with PBST, the embryos were incubated with Alexa Fluor 555 Goat anti-mouse IgG (H + L) Antibody (1:800) and Alexa Fluor 488 Goat anti-rabbit IgG (H + L) Antibody (1:800). The embryos were washed and mounted using 70% glycerol and pictures were taken by a confocal microscope. Three independent experiments were performed.

TUNEL assay

TUNEL staining was performed with Tg(*runx1:en-GFP*) zebrafish embryos at 48 hpf, 52 hpf and 60 hpf using the *In Situ* Cell Death Detection Kit (Roche). The samples were imaged using a confocal microscope. Three independent experiments were performed.

RNA immunoprecipitation sequencing (RIP-seq), RIP-qPCR and m⁵C RIP-qPCR

RIP was performed as described previously.²² Tg(*hsp70:flag-ybx1-EGFP*) embryos were heat shocked at 42°C for 30 min at 36 hpf. The EGFP⁺ and EGFP⁻ embryos were collected at 52 hpf as experimental group and control group, respectively. The tail region of zebrafish embryos for each sample ($n = 1000$) were lysed in lysis buffer (150 mM KCl, 10 mM HEPES, 2 mM EDTA, 0.5% NP40, 0.5 mM DTT, proteinase inhibitor, RNasin) and were pre-cleared with Dynabeads protein A (Invitrogen). 50 µL pre-cleared lysate was spared for Input. Then the remaining lysate was incubated with Anti-Flag M2 Affinity Gel (Invitrogen). After washed with ice-cold NT2 buffer (200 mM NaCl, 50 mM HEPES pH 7.6, 2 mM EDTA, 0.05% NP-40, 0.5 mM DTT, 0.4 U/ml RNase inhibitor) and following ice-cold MN buffer (50 mM Tris-HCl pH 7.9 and 5 mM CaCl₂), the RNA was fragmented with MNase (2 U/ml, NEBuilder) in MN buffer and washed with ice-cold PK buffer (100 mM Tris-HCl pH 7.4, 50 mM NaCl, 10 mM EDTA, 0.2% SDS). Treated with proteinase K (4 mg/mL, Roche) in PK buffer, the RNA was purified, and ethanol precipitated. The extracted RNA was subjected to RNA-seq library construction. RIP-seq experiments were conducted with two independent experiments.

For Flag-Ybx1 RIP-qPCR and Flag-Pabpc1a RIP-qPCR, RIP was performed according to procedure mentioned above. For m⁵C RIP-qPCR, 5 µg anti-m⁵C antibody (Active Motif) or anti-IgG antibody (Beyotime) were incubated with Dynabeads Protein A

(Invitrogen) in IPP buffer (150 mM NaCl, 0.1% NP-40, 10 mM Tris-HCl, pH 7.4, 0.4 U/ml RNase inhibitor). 1/10 Flag-Ybx1 immunoprecipitated RNA was spared for Input. Then, an equal amount of Flag-Ybx1 immunoprecipitated RNA (500 ng) was incubated with the anti-m⁵C antibody-beads and anti-IgG antibody-beads, respectively. After washed with IPP buffer, RNA was extracted.

Input and immunoprecipitated RNA were reversely transcribed using RevertAidTM First Strand cDNA Synthesis kit (Invitrogen) and used for further qPCR with SYBR Green (TIANGEN) on QuantStudio3 Real-Time PCR system (Thermo Fisher). The relative enrichment of Ybx1, IgG and m⁵C was analyzed by normalizing to the Input. RIP-qPCR experiments were conducted with three independent experiments.

Primer sequences used are listed in [Table S1](#).

Pull-down assay

HA-ybx1 mRNA-injected embryos were lysed with lysis buffer (50 mM Tris-HCl pH 7.5, 350 mM NaCl, 0.4 mM EDTA, 1% NP-40, 1 mM DTT, 0.4 U/ml RNase inhibitor) and pre-cleared for 1 h at 4°C with streptavidin-conjugated magnetic beads, which were washed with binding buffer (50 mM Tris-HCl pH 7.4, 150 mM NaCl, 0.5 mM EDTA, 0.1% NP-40, 1 mM DTT, protease inhibitor cocktail, RNase inhibitor). The pre-cleared embryo lysate (1/10 was spared for Input) and pre-cleared streptavidin-conjugated magnetic beads (incubation with 0.2 mg/mL tRNA (Sigma-Aldrich) and 0.2 mg/mL BSA (NEBuilder) for 1 h at 4°C) were incubated together with biotin-labeled RNA oligonucleotides (pre-heated for 5 min at 65°C) at 4°C for 2 h. After washing, the beads-oligo-protein mixture was heated with NuPAGE LDS Sample Buffer (4×) (Invitrogen) and separated by NuPAGE 4%-12% Bis-Tris Gel (Invitrogen). For pull-down assay in HEK293T cells, pCS2+*-HA-ybx1*^{WT} and pCS2+*-HA-ybx1*^{W45F} plasmid were transfected into HEK293T cells. After harvested, the transfected cells were treated following the procedures mentioned above. The pull-down assays were conducted with three independent experiments.

mRNA stability analysis

The α-amanitin is an RNA polymerase II inhibitor. α-amanitin treatment leading to transcription inhibition, we can evaluate the mRNA stability by calculating the remaining mRNA level.^{36,37} 0.2 ng α-amanitin (Sigma-Aldrich) was injected into the yolk sac of 52 hpf embryos. The CHT region of injected embryos (*n* = 30) was collected at indicated time points for RNA extraction using Trizol Reagent (Invitrogen). The remaining RNA level was determined by qPCR and normalized to the 0 h post injection values. Three independent experiments were performed.

m⁵C reporter assay

The m⁵C reporter constructs were generated by inserting EGFP-fused wild type (WT) (containing m⁵C site) or mutant (MUT) (cytosine with m⁵C site was synonymously replaced) of target (coding sequences) CDS into the pCS2+ vector. In detail, the *cyclin d1* CDS contains a single m⁵C modification site (cytosine at position 829 from the start codon), which was synonymously mutated from GAC to GAT (both encoding Asp) to generate the *cyclin d1* MUT plasmid. *mcm6* CDS contains a single m⁵C modification site (cytosine at the position 959 from the start codon), which was synonymously mutated from CCC to CCA (both encoding Pro) to generate the *mcm6* MUT plasmid. The plasmids were linearized and transcribed into mRNA using mMessage mMachine SP6 kit (Invitrogen). 200 pg WT or MUT mRNA and 100 pg tdTomato mRNA were injected into 1-cell stage embryos. At 50% epiboly stage, photos were taken to record the fluorescence intensity and embryos were collected for RNA extraction following qPCR. tdTomato served as injection control.

Confocal microscopy

For living transgenic zebrafish embryos, the fish were dechorionated and placed in 1% low-melting-point agarose. For the time-lapse imaging of HSPC divisions, the mounted control MO and *ybx1* MO with Tg(*kdr1*:mCherry;*runx1*:en-GFP) background were taken pictures at 46 hpf. For embryos after FISH, EdU and pHH3 staining, TUNEL, the fish were placed on a microscope slide and sealed by a cover glass. Photos were taken by Andor Dragonfly 505 confocal microscope (Oxford Instruments). Images were further edited using ImarisViewer.

UHPLC-MS/MS analysis of m⁵C levels

Total RNA was extracted from tail region of zebrafish embryos at 60 hpf with TRIzol (Invitrogen). mRNA enrichment was performed with the mRNA Capture Beads (Vazyme). For m⁵C detection, mRNA sample was subjected to ultra-high performance liquid chromatography coupled to mass spectrometry (UHPLC-MS/MS) analysis, following previously established method.¹⁹ Three independent experiments were performed in triplicate.

Flow cytometry for mouse fetal liver cells

Single-cell suspensions from the mouse fetal liver were prepared by mechanical dissociation, and the cells were stained for 30 min at 4°C. Antibodies used in this study included those against: FITC anti-mouse Lineage (BioLegend), APC anti-mouse CD117 (eBioscience), PE-Cyanine7 anti-mouse Ly-6A/E (eBioscience). Viability staining solution was used to exclude dead cells. Ki67 antibody was tested by intracellular staining using the Staining Buffer Set (Fixation/Permeabilization Buffer). Flow cytometry was performed using Invitrogen Bigfoot, and the analysis was carried out with Flowjo (v10.8.1). Three independent experiments were performed.

Small Interference RNA (siRNA) transfection

Control and target gene siRNAs were designed (Table S1) and synthesized by Genepharma Corporation. Lineage⁻Sca-1⁺c-Kit⁺ (LSK) cells were sorted from E14.5 FLs, cultured in medium [SFEM, and cytokine cocktail (SCF, Flt3L, IL-6, and TPO)] and transfected with siRNAs using LipofectamineTM RNAiMAX Transfection Reagent (Invitrogen, 13778030) according to the manufacturer's instructions. After 72h, the cells were sorted for CFU assay, western blot, cell culture and qPCR.

Colony-forming unit (CFU) assay

RNAiMAX-infected cells were harvested by mechanical pipetting for generating single-cell suspensions. Then, the single-cell suspensions were added into MethoCult GF M3434 medium (STEMCELL Technologies, 03434) in ultra-low attachment 24-well plates (Costar). The cells were cultured at 37°C with 5% CO₂ or under hypoxic conditions for 7–10 days for colony quantification. Subsequently, the number of each type of colony, including CFU-E, CFU-GM, and CFU-GEMM, was counted based on morphology. Three groups of independent experiments were analyzed. CFU-E, CFU-erythroid; CFU-GEMM, CFU-granulocyte, erythrocyte, macrophage, megakaryocyte; CFU-GM, CFU-granulocyte, macrophage.

HSPC cell culture

RNAiMAX-infected cells were cultured in medium [SFEM, and cytokine cocktail (SCF, Flt3L, IL-6, and TPO)] for 4 days. Then cells were sorted for flow cytometry analysis and qPCR.

RNAiMAX-infected cells were cultured with α-amanitin treatment, then, the cells were harvested at 0h, 4h, 8h, 12h, 24h for qPCR analysis.

Cell sorting, RNA preparation, and mRNA purification

For CD41:GFP transgenic line, the GFP-positive cells were divided into CD41:GFP^{low} and CD41:GFP^{high} populations based on fluorescence intensities on the FACS since they were identified as HSPCs and thrombocytes, respectively.⁷⁶ 1×10⁵ CD41:GFP^{low} cells from the trunk region of wild type embryos at 33 hpf, the CHT region of control and *ybx1* morphants at 52 hpf were sorted by FACS. 1×10⁵ *runx1*:en-GFP⁺ cells from kidney marrow of wild type zebrafish at 12 mpf were sorted by FACS. Total RNA isolated by TRIzol (Invitrogen), ethanol precipitation, and DNase I (NEBuler) digestion was used for further library preparation and RNA sequencing.

8–10×10⁵ CD41:GFP^{low} cells from trunk region of wild type embryos at 33 hpf and tail region of wild type embryos at 52 hpf and 8–10×10⁵ *runx1*:en-GFP⁺ cells from kidney marrow of wild type zebrafish at 12 mpf were sorted by FACS. Total RNA isolated by TRIzol (Invitrogen), ethanol precipitation, and DNase I (NEBuler) digestion was used for further library preparation and RNA bisulfite sequencing. Two biological replicates at each developmental stage were generated for RNA-seq or RNA-BisSeq.

RNA-seq and RNA-BisSeq library preparation

Library preparation for RNA-seq was carried out according to the instructions of KAPA Stranded mRNA-Seq Kit (KAPA). The preparation of RNA-BisSeq libraries was conducted following a previous study.²² Mouse *Dhfr* mRNA served as a methylation conversion control. A mixture of 200 ng mRNA and *Dhfr* mRNA at a ratio of 300:1 was fragmented into 100 nt fragments for 1 min at 90°C using 10×RNA fragmentation reagent (Ambion) and stopped with 10×RNA stop solution (Ambion). After ethanol precipitation, the RNA was treated in 100 μL bisulfite solution (pH 5.1) and incubated for 1 h at 75°C. The reaction mixture was then desalting by centrifugation through Nanosep with 3K Omega 500/pk columns (PALL Corporation). The RNA was washed with nuclease-free water for five times and dissolved in 100 μL nuclease-free water following incubation with 100 μL 1 M Tris-HCl (pH 9.0) for 1 h at 75°C. Precipitated with ethanol, the RNA was dissolved and reverse transcribed using superscript II Reverse Transcriptase (Invitrogen) and ACT random hexamers. The procedures were performed following the instructions of KAPA Stranded mRNA-Seq Kit (KAPA).

High-throughput sequencing data processing

RNA-seq, RIP-seq, and RNA-BisSeq were carried out on Illumina NovaSeq 6000 platform with paired-end 150 bp read length. Cutadapt (version 1.13)⁷⁷ was used to remove sequencing adaptors. Trimmomatic (version 0.33)⁷⁸ was used to filter out reads with length <35 nt and of low quality to get clean reads.

For RNA-seq analysis, clean reads were mapped to the zebrafish genome (version zv10) using Hisat2 (version 2.0.5)⁷⁹ and uniquely mapped reads with a quality score ≥20 were kept for subsequent analysis. The number of reads mapped to each transcript was counted using featureCounts (version 1.6.2, parameters: -t exon -g gene_id -p -s 2 -Q 20),⁸⁰ and the RPKM (reads per kilobase of exon model per million mapped reads) was calculated for each gene. The changes in gene expression identified in zebrafish HSPCs after *ybx1* deficiency are listed in Table S2.

For RIP-seq analysis, genome mapping of RIP-seq data was conducted in the same way as for RNA-seq. Peak calling was performed using MACS2 (version 2.1.4)⁸¹ with the parameters: --keep-dup all -f BAM --nomodel -g 1369631918 -B -p 0.05 based on replications. Peak annotation was implemented using BEDTools (version 2.28.0).⁸² The information of binding targets is listed in Table S3.

To identify the down-regulated *Ybx1* binding targets, we integrated RNA-seq derived from both control samples and those treated with *ybx1* MO, alongside *Ybx1* RIP-seq. 198 mRNAs were bound by *Ybx1* and showed down-regulated expression upon *ybx1* deficiency.

For RNA-BisSeq analysis, clean reads were aligned to the zebrafish genome (zv10) using meRanGh align (meRanTK, version 1.2.1)⁸³ with the following parameters: -fmo -mmr 005. The C-to-T conversion rate was evaluated using *Dhfr*. Only mapped reads with a conversion rate >99% in the sample were retained for further m⁵C sites calling using meRanCall (meRanTK, version 1.2.1)⁸³ with the following parameters: -mBQ 20 -mr 0. The methylation level was calculated as previously reported.²² Only sites with methylation level ≥ 0.1 , coverage depth ≥ 30 and methylated cytosine count ≥ 5 were retained. Additionally, in order to further reduce the false-positive sites, multiple m⁵C sites that appeared within 10-bp reads were eliminated. The sites screened in each replication were merged for downstream analysis. BEDTools (version 2.28.0)⁸² was used for sites annotation. The m⁵C sites identified in zebrafish HSPCs are listed in Table S4.

Differential expressed gene (DEG) analysis

The DEG analysis was performed using the R package edgeR,⁸⁴ and the genes with |Fold change| ≥ 1.5 and *p* value < 0.05 were considered as statistically significant.

Dynamic changes of RNA m⁵C between adjacent stages

To compare the dynamic changes of RNA m⁵C between adjacent developmental stages in HSPCs, the total methylation level of each mRNA (the cumulative value of the methylation level across all the m⁵C sites per mRNA) was calculated. mRNAs displaying a methylation level ≥ 0.2 were considered as differentially methylated mRNAs (DM-mRNAs).²² To further evaluate the effects of dynamic m⁵C modifications on mRNA stability, the abundance changes of DM-mRNAs between consecutive stages were compared with cumulative distribution functions.

RNA abundance changes of m⁵C-modified mRNAs after *ybx1* deficiency

All expressed cell cycle-related mRNAs in CHT-resident HSPCs were divided into two groups: with and without m⁵C modification. The abundance changes of these two groups of mRNA upon *ybx1* deficiency were compared based on the DEG analysis results. The significance evaluated by *p* value was calculated using Wilcoxon test.

Distribution patterns analysis of Ybx1 targets and m⁵C peaks

The distribution pattern along transcripts analysis of Ybx1 target and m⁵C was performed using an in-house script. Briefly, Ybx1 binding regions and m⁵C sites were annotated to exons by BEDTools (version 2.28.0),⁸² and their distribution densities were calculated based on their relative positions within the 5'UTR, CDS and 3'UTR.

The relationship between Ybx1 targets and m⁵C sites was performed by calculating the distances between Ybx1 target regions or random sequences and m⁵C sites. The random sequences were selected with the same counts and length as the Ybx1 target regions. Through comparing with the random regions, the relationship between Ybx1 targets and m⁵C sites could be determined.

Gene ontology (GO) analysis

DAVID (version 6.8)⁸⁵ was used to perform GO analysis. GO terms with *p* < 0.05 were considered as statistically significant. The Gene-Concept Network was performed by R using enrichGO and cnetplot functions. The downregulated m⁵C-modified Ybx1 targets upon *ybx1* deficiency were set as input.

Function network analysis

Cytoscape (version 3.8.0)⁸⁶ was used to generate the function network diagram by EnrichmentMap for visualization. The cutoff of Q value and *p* value were both set as 0.05, and the Edge Cutoff was set as 0.5.

Gene Set Enrichment Analysis

Gene Set Enrichment Analysis (GSEA) was performed by R for interpreting differential regulatory pathways upon *ybx1* deficiency. The log₂(Fold Change) value of Ybx1-targeted mRNAs obtained through differentially expression analysis with the R package edgeR⁸⁴ were sorted in descending order and used as input. Using the R package clusterProfiler,⁸⁷ the GSEA function was used for functional enrichment analysis of the input mRNAs, and enrichment entries with *p* < 0.05 were considered as significant. Negative running enrichment score (NES) indicated that the corresponding function was down-regulated upon *ybx1* deficiency.

QUANTIFICATION AND STATISTICAL ANALYSIS

The statistical analysis of qPCR, confocal microscopy and WISH results were performed at least three independent biological replicates. WISH signals were analyzed by ImageJ to calculate signal intensities according to a previous study.⁸⁸ The HSPC number of confocal images was calculated by using the spots model of software Imaris X64.9.3.1. All of the statistical data are shown as mean \pm SD and analyzed using Graph Pad Prism 6 software, unless otherwise specified in the figure legends or STAR Methods. The *p* values were determined using a two-tailed unpaired Student's *t*-test, unless otherwise specified in the figure legends or STAR Methods. ns: no significance, **p* < 0.05; ***p* < 0.01; ****p* < 0.001; *****p* < 0.0001.